

Article

https://doi.org/10.1038/s41593-025-02066-2

Hormonal milieu influences whole-brain structural dynamics across the menstrual cycle using dense sampling in multiple individuals

Received: 13 December 2023

Accepted: 19 August 2025

Published online: 26 September 2025

Check for updates

Carina Heller ^{1,2,3,4,5,6,24} , Daniel Güllmar^{7,24}, Lejla Colic ^{1,5,6}, Laura Pritschet ⁸, Martin Gell^{2,9,10}, Nooshin Javaheripour¹, Feliberto de la Cruz ¹¹, Philine Rojczyk^{12,13}, Carina J. Koeppel ^{5,14}, Bart Larsen ^{2,3,15}, Habib Ganjgahi^{16,17}, Frederik J. Lange¹⁸, Ann-Christine Buck¹⁹, Tim L. Jesgarzewsky¹⁹, Robert Dahnke²⁰, Michael Kiehntopf²¹, Emily G. Jacobs ^{4,22}, Zora Kikinis¹³, Martin Walter^{1,5,6}, Ilona Croy^{5,6,19,23} & Christian Gaser ^{1,5,6,20}

Gonadal hormone receptors are widely distributed across the brain, yet their influence on brain structure remains understudied. Here, using precision imaging, we examined four females, including one with endometriosis and one using oral contraceptives (OC), across a monthly period. Whole-brain analyses revealed spatiotemporal patterns of brain volume changes, with substantial variations across the monthly period. In typical cycles, spatiotemporal patterns were associated with serum progesterone levels, while in cycles with endometriosis and during OC intake, patterns were associated with serum estradiol levels. The volume changes were widely distributed rather than region-specific, suggesting a widespread but coordinated influence of hormonal fluctuations. These findings underscore the importance of considering diverse hormonal milieus beyond typical menstrual cycles in understanding structural brain dynamics and suggest that hormonal rhythms may drive widespread structural brain changes.

Physiological fluctuations in levels of gonadal hormones, such as endogenous estradiol and progesterone, orchestrate the rhythm of the female menstrual cycle throughout the reproductive years^{1,2}. The typical menstrual cycle spans 25–32 days, beginning with the follicular phase characterized by menses, followed by a rise in estradiol levels alongside low progesterone concentrations; around cycle day 14, ovulation marks the transition into the luteal phase, marked by rising progesterone levels and a second peak in estradiol, and then followed by a decline in both hormones toward the end of the cycle³. Ex vivo animal data have shown a widespread distribution of both progesterone and

estradiol receptors throughout the brain, with varying expression levels depending on the specific brain region. While brain structures typically associated with the limbic system (for example, thalamus, hippocampus, amygdala and hypothalamus) are richer in estrogen and progesterone receptors, these receptors are also expressed, albeit to a lesser extent, in the cerebral and cerebellar cortex 4,5 . Estradiol and progesterone have pivotal roles in synaptogenesis, myelination processes and the modulation of spine density $^{6-11}$. As such, these hormones have potential to modulate brain structure, function, chemistry $^{12-14}$ and, by extension, to influence behavior 11 . This is further demonstrated by hormonal

A full list of affiliations appears at the end of the paper. —e-mail: carina.heller@uni-jena.de

influences on cognition, memory $^{15-18}$, stress responsiveness $^{19-21}$ and mood regulation $^{22-25}$. While animal studies have provided valuable insights into the role of gonadal hormones on the brain, they often focus on a limited number of regions (for example, hippocampus). However, given that estradiol and progesterone receptors are expressed across the entire brain, a whole-brain approach is essential to better understand the broader impact of these hormones. Because these hormones can modulate brain structure, examining the entire brain would offer a deeper understanding of their effects on neural dynamics.

Studies investigating the effect of endogenous hormones on brain neuroplasticity in vivo in human neuroscience often involve collecting data from multiple individuals at a single time point to establish mean comparisons and average hormone–brain associations. This cross-sectional method, such as comparing females in the follicular versus the luteal phase, has identified differences in global gray matter volume²⁶ as well as region-specific differences (for example, hippocampus^{27,28}, parahippocampal gyrus^{28,29}, middle frontal gyrus^{27,30} and cerebellum²⁸). However, this method overlooks the rhythmic nature of hormone production within the body. Furthermore, averaging across participants may obscure individual differences, warranting a personalized (within-participant) analysis.

Recent years have witnessed a paradigm shift in neuroimaging studies, with an alternative approach that involves the longitudinal tracking of individual participants over extended periods of weeks and months, increasing the sensitivity to detect associations among fluctuations in gonadal hormones and brain structure^{31,32}. An emerging trend has centered on the comprehensive monitoring of the female menstrual cycle over time periods ranging from days to weeks and months, aiming to enhance our understanding of hormone-induced effects within the human brain³³⁻⁴⁰. This approach has enriched our insights into the multifaceted impact of hormones on human brain function and structure by detecting subtle changes that could be overlooked in less frequent sampling. Densely sampled neuroimaging studies tracking a single individual across a complete menstrual cycle have primarily focused on investigating functional networks and connectivity^{33,35-38}. Only two densely sampled neuroimaging studies have examined structural changes, exclusively within regions of interest (hippocampus and medial temporal lobe^{39,40}). In the most recent investigation, 27 female participants underwent six scans throughout their menstrual cycle. Here the authors reported associations among plasma estradiol levels, progesterone levels and subfield volumes within the hippocampus⁴¹. While region-specific analyses reveal how particular brain areas differ across the menstrual cycle, they do not provide insights into the dynamic changes that occur throughout the brain. Adopting a whole-brain approach would provide a broader perspective on the range of brain structures that change across the full menstrual cycle in response to day-to-day hormonal fluctuations.

To expand our understanding of the impact of estradiol and progesterone on the brain's structure, it is essential to expand the scope of our research beyond individuals with typical menstrual cycle patterns. Including participants with endocrine disorders such as endometriosis, a condition characterized by a unique hormonal profile42-44, will provide a more nuanced understanding of the complex interplay between gonadal hormones and their influence on brain structure. Endometriosis, a chronic and inflammatory gynecological disorder, affects approximately 10-15% of females in their reproductive years 45. It is defined by the presence and growth of ectopic endometrial stroma and glands outside the uterine cavity, typically within the peritoneal cavity. This pathological phenomenon can have various clinical manifestations, including chronic pelvic pain, dysmenorrhea, dyspareunia and infertility46,47. The condition is accompanied by hormonal dysregulations-the development, growth and maintenance of endometriotic lesions are driven and sustained by endogenous estrogen, and endometriosis is associated with an increased estradiol synthesis and decreased inactivation, resulting in elevated local concentrations of this hormone, referred to as estrogen dependency^{42,43,48–50}. In parallel, the endometriotic lesions can become resistant to the inhibitory actions of endogenous progesterone, known as progesterone resistance⁴⁴; consequently, even in the presence of progesterone, these tissues may continue to grow, bleed and cause inflammation rather than responding with the typical growth suppression seen in healthy endometrial tissue^{51–53}.

The current study used four densely sampled females who underwent extensive and standardized brain imaging and venipuncture throughout their entire menstrual cycle. Using a whole-brain approach, we aimed to delineate individualized trajectories of structural brain patterns and to investigate the impact of endogenous day-to-day hormone fluctuations on these trajectories. Similar to the principles of whole-brain functional connectivity analyses, which probe the interactions and communication between different regions, we aim to understand how the brain changes as a whole across the menstrual cycle. Through this approach, we seek to elucidate the influence of hormonal fluctuations on the entire brain, offering nuanced insights into the dynamic processes of hormone-induced neuroplasticity.

To investigate neurostructural dynamics across hormonal states, we conducted a dense-sampling study involving multiple participants. First, we densely sampled a healthy female with a typical menstrual cycle, referred to as 'typical cycle' (Extended Data Fig. 1a). We then leveraged the densely sampled open-access 28andMe dataset of another female^{33-38,40}. This dataset will be referred to as '28andMe (typical) cycle' (Extended Data Fig. 1b). To extend the relevance of our findings and to probe the neural effects of hormonal dysregulation, we repeated these procedures in a female participant diagnosed with endometriosis. This dataset will be referred to as 'endometriosis cycle' (Extended Data Fig. 1c). Additionally, we included one female using oral contraceptives (OC), characterized by substantially suppressed endogenous serum progesterone levels, and estradiol levels comparable to a natural cycle. This dataset will be referred to as 'OC cycle' (Extended Data Fig. 1d). We first compared endogenous gonadal hormones-serum estradiol levels, serum progesterone levels and their ratio-among the four individuals to evaluate the presence of hormonal dysregulation in the female with endometriosis. Then, using singular value decomposition (SVD) analyses, we generated whole-brain volumetric (VSTPs) and cortical thickness spatiotemporal patterns (CSTPs) across the monthly period. After this, we investigated the potential association between these patterns and gonadal hormones within each individual. Subsequently, voxel-wise and vertex-wise analyses were used to directly link the hormonal fluctuations to structural brain measures. To further contextualize our results, we repeated the study procedure and acquired an additional dense-sampling dataset from one male over a comparable monthly period, during which no specific gonadal hormone patterns were expected.

In this study, we use the term 'females' instead of 'women' to emphasize the biological aspect, focusing on biological sex rather than gender. It is worth noting that language regarding these terms is constantly evolving. We emphasize that sex hormones represent crucial biological factors in the human experience, transcending any perceived binaries.

Results

Endocrine assessments and menstrual cycle patterns

Gonadal hormones were assessed throughout the full menstrual cycle (Fig. 1a). Analyses of hormone serum concentrations in the typical cycle and the 28 and Me (typical) cycle confirmed the expected rhythmic changes of a natural menstrual cycle. In the typical cycle, the 25 test sessions covered 15 days of the follicular phase and 10 days of the luteal phase. In the 28 and Me (typical) cycle, the 30 test sessions covered 14 days of the follicular phase and 16 days of the luteal phase. The ratios between progesterone and estradiol concentrations suggested a typical hormonal balance during the luteal phase.

a Hormone concentrations across cycles

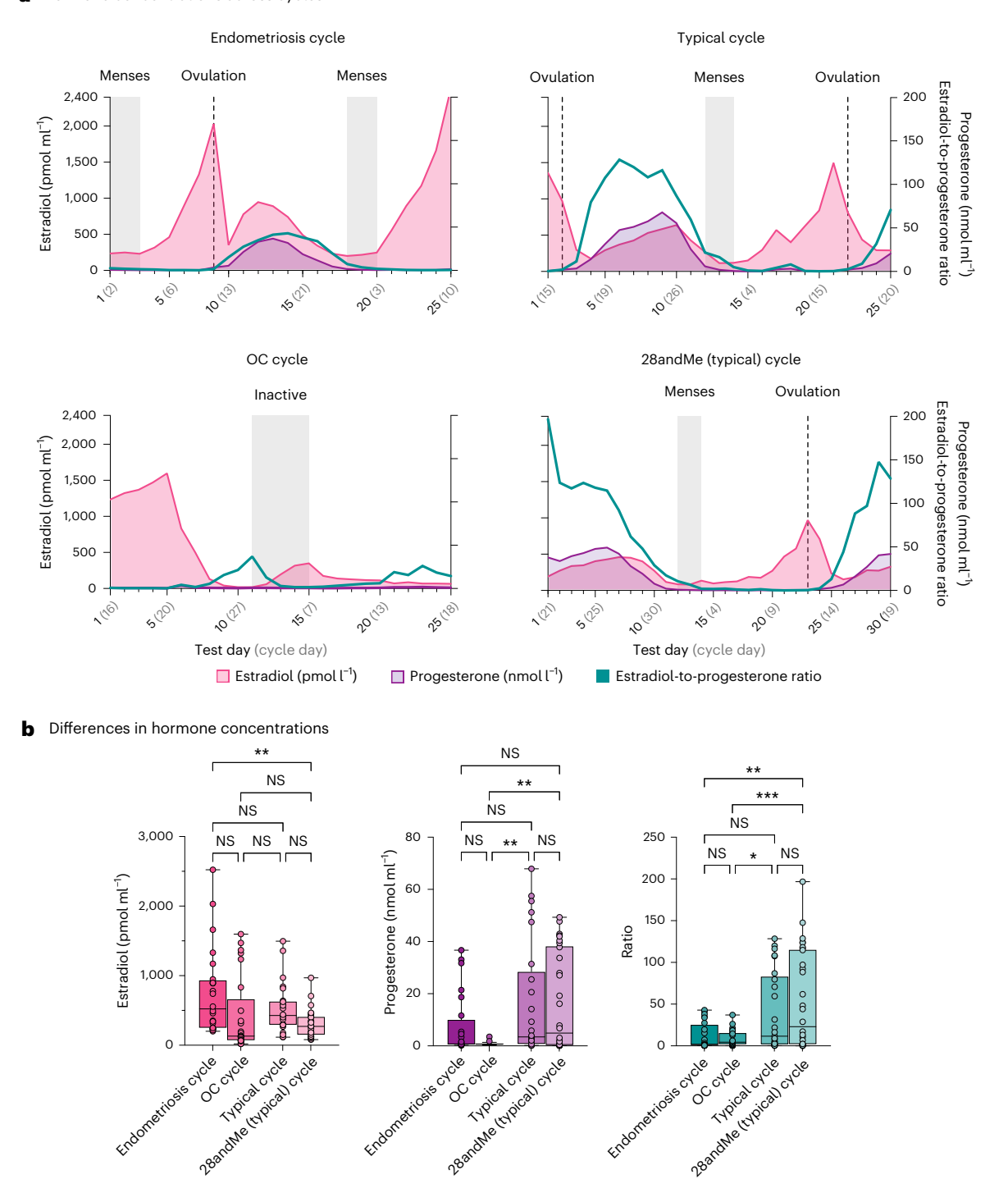


Fig. 1 | Hormone concentrations of estradiol, progesterone and the estradiol-to-progesterone ratio for female participants (n=4). a, Hormones concentrations across the test sessions for female participants (n=4). Solid lines and colored shaded areas represent hormonal levels; gray shading indicates menses in typical cycles and the endometriosis cycle, and inactive pill phase in the oral contraceptives (OC) cycle; dotted lines indicate ovulation. Hormone levels indicate a typical hormonal balance in the typical and 28 and Me (typical) cycles, while hormone levels in the endometriosis and OC cycles suggest estradiol dominance. b, To test whether hormonal profiles differed among the

four individuals, a one-way MANOVA was conducted, followed by a post hoc ANOVAs, and two-sided post hoc t-tests. The box-and-whisker plots show the median (centerline), upper and lower quartiles (box), minimum and maximum values (whiskers); individual points are shown. Asterisks indicate significance level (***P < 0.001, **P < 0.01, *P < 0.05) based on two-sided post hoc t-tests with Bonferroni correction for multiple comparisons. For exact P values, see Main. Graphs were created with GraphPad Prism (version 10). NS, nonsignificant; MANOVA, multivariate analysis of variance; ANOVAs, analyses of variance.

In the endometriosis cycle, gonadal hormone concentrations also followed the rhythmic changes of a menstrual cycle. The 25 test sessions covered 17 days of the follicular phase and 8 days of the luteal

phase. As predicted, the estradiol-to-progesterone ratio suggested an estradiol dominance during the luteal phase. The menstrual cycles covered in the participant with endometriosis lasted 23 and 24 days

respectively during the experiment, representing shorter menstrual cycles (\leq 24 days)—a typical feature of endometriosis. In the OC cycle, circulating progesterone levels were selectively suppressed. The concentration and dynamic range of estradiol during the oral contraception intake were similar to those observed in a typical menstrual cycle. Estradiol-to-progesterone ratios suggested an estradiol dominance, providing an additional dataset with a hormonal milieu similar to that of the endometriosis cycle.

Progesterone concentrations surpassed 15.9 nmol l⁻¹ in the typical, 28andMe (typical) and endometriosis cycle, suggesting an ovulatory cycle⁵⁴.

To test whether hormonal profiles differed between participants, a one-way multivariate analysis of variance was conducted with serum estradiol levels, progesterone levels and the estradiol-to-progesterone ratio as dependent variables, and the four individuals (typical cycle, 28andMe (typical) cycle, endometriosis cycle and OC cycle) as fixed factors. The analysis revealed a significant main effect among the four individuals (Pillai's trace, $F_{(9,300)} = 4.52$, $P < 0.001 \eta^2 = 0.12$; Roy's largest root, $F_{(3,100)} = 10.14$, P < 0.001, $\eta^2 = 0.23$). Post hoc analyses of variance indicated significant differences among the four individuals in estradiol levels ($F_{(3.100)} = 4.70$, P = 0.004, $\eta^2 = 0.12$), progesterone $(F_{(3,100)} = 5.94, P < 0.001, \eta^2 = 0.15)$ and the estradiol-to-progesterone ratio $(F_{(3.100)} = 7.83, P < 0.001, \eta^2 = 0.19)$. Post hoc two-tailed *t*-tests, corrected using the Bonferroni method, further revealed that the endometriosis cycle had significantly higher estradiol levels compared to the 28 and Me (typical) cycle (P = 0.002), and that progesterone levels were significantly lower in the OC cycle compared to the typical cycle (P=0.005) and the 28andMe (typical) cycle (P=0.003). The endometriosis cycle also showed a significantly lower estradiol-to-progesterone ratio compared to the 28 and Me (typical) cycle (P = 0.002), and the OC showed lower estradiol-to-progesterone ratios compared to both the typical cycle (P = 0.045) and the 28andMe (typical) cycle (P < 0.001). Differences in hormonal values are displayed in Fig. 1b.

Whole-brain structural dynamics

 $T_1\text{-weighted}$ (T1w) images were acquired from each participant across the full menstrual cycle—five consecutive weeks for the typical cycle, the endometriosis cycle and the OC cycle, and four consecutive weeks for the 28andMe (typical) cycle. Preprocessing was performed using SPM12 (http://www.fil.ion.ucl.ac.uk/spm) and CAT12 toolbox (https://neuro-jena.github.io/cat) 55 with the longitudinal pipeline approach. Each processed T1w image represents a snapshot of brain structure on each test day. Next, SVD analysis was used to extract VSTPs and CSTPs. SVD decomposed the images into spatiotemporal components, reflecting patterns of brain structure over time. To capture shared spatial patterns across individuals, data from all cycles (typical, 28andMe (typical), endometriosis and OC cycle) were concatenated.

In SVD, eigenvalues represent the variance explained by each principal component, while eigenvectors represent the temporal patterns. Warm colors in the spatial components denote positive associations with the eigenvectors of the temporal component, indicating that these regions increase as the corresponding temporal pattern increases. Cool colors signify negative associations, meaning these regions decrease as the temporal pattern increases. These patterns are referred to as 'spatiotemporal patterns'. It is important to note that the values derived from the SVD (eigenvalues and eigenvectors) are arbitrary in magnitude, meaning they lack an inherent unit of measurement but are used to identify patterns of association. A schematic illustration of the workflow is shown in Fig. 2.

Volumetric dynamics. In the volumetric analysis (Fig. 3a), VSTP1 explained 47.7% of the variance, with the most substantial clusters spanning the gray matter of the cerebellum, precuneus, middle frontal gyrus, lingual gyrus, angular gyrus and temporal gyrus. VSTP2 explained 20.4% of the variance, with the most substantial clusters

overlapping with the gray matter of the cerebellum, thalamus, temporal gyrus, precentral gyrus and gyrus rectus. VSTP3 explained 9.7% of the variance, with the most substantial clusters located in the gray matter of the cerebellum, superior and middle frontal gyrus, supplementary motor cortex, precuneus, precentral gyrus and thalamus (Supplementary Table 1). All other VSTPs explained less than 10% of the variance and were excluded from further analyses.

Generalized additive models (GAMs) were used to analyze changes in the extracted spatiotemporal patterns across the monthly period. This choice was motivated by its ability to capture potential nonlinear trends, including curvature and variations in change rates, that are often present in the longitudinal data. VSTP1, VSTP2 and VSTP3 were found to significantly fluctuate across all four participants (Fig. 4 and Supplementary Table 2).

Hormonal associations with volumetric dynamics. To assess whether the short-term VSTPs were driven by fluctuations in gonadal hormones, time-series regression analyses were used. Serum estradiol levels, progesterone levels and the estradiol-to-progesterone ratio were separately specified as independent variables for each individual and spatiotemporal pattern. Because not all variables were normally distributed, relationships were further modeled using nonparametric functional Spearman rank correlation. Results were highly consistent across both approaches.

In the typical cycle, both progesterone levels ($\beta = 0.021$, $P_{\text{FDR}} = 0.010$) and the estradiol-to-progesterone ratio ($\beta = 0.015$, $P_{\rm FDR}$ = 0.007) were significantly associated with VSTP1, with corresponding significant Spearman correlations (progesterone, ρ = 0.642, P_{FDR} = 0.005; estradiol-to-progesterone ratio, ρ = 0.587, P_{FDR} = 0.011). Similarly, for the 28andMe (typical) cycle, progesterone levels (β = 0.017, $P_{\rm FDR}$ < 0.001) and the estradiol-to-progesterone ratio (β = 0.011, P_{FDR} < 0.001) showed positive associations with VSTP1, again with corresponding significant Spearman correlations (progesterone, ρ = 0.586, P_{FDR} = 0.002; estradiol-to-progesterone ratio, $\rho = 0.693$, $P_{\text{FDR}} < 0.001$). Additionally, progesterone levels ($\beta = -0.044$, $P_{\rm FDR}$ < 0.001) and the estradiol-to-progesterone ratio (β = -0.025, $P_{\rm FDR}$ < 0.001) were significantly negatively associated with VSTP2 $(P_{EDR} < 0.001)$, supported by corresponding negative Spearman correlations (progesterone, $\rho = -0.631$, $P_{\text{FDR}} < 0.001$; estradiol-to-progesterone ratio, $\rho = -0.592$, $P_{\text{FDR}} = 0.002$). Estradiol levels were significantly associated with VSTP3 only in the 28 and Me (typical) cycle (β = 0.003, P_{FDR} < 0.044), supported by a corresponding Spearman correlation $(\rho = 0.571, P_{FDR} = 0.002).$

In the endometriosis cycle, estradiol levels were significantly associated with VSTP1 (β = 0.006, $P_{\rm FDR}$ = 0.010), with a corresponding significant Spearman correlation (ρ = 0.571, $P_{\rm FDR}$ = 0.037). No significant relationships were observed for VSTP2 or VSTP3. Similarly, in the OC cycle, estradiol levels showed a significant association with VSTP1 (β = 0.006, $P_{\rm FDR}$ = 0.023). Additionally, the estradiol-to-progesterone ratio was significantly negatively associated with VSTP1 (β = -0.037, $P_{\rm FDR}$ = 0.046) and VSTP2 (β = -0.021, $P_{\rm FDR}$ = 0.046). However, Spearman correlations in the OC cycle did not remain significant after false discovery rate (FDR) correction. No significant associations were observed for VSTP3. Progesterone levels did not exhibit significant associations in either the endometriosis or the OC cycle (Fig. 4). All results are displayed in Supplementary Table 3.

Cortical thickness dynamics. In the cortical thickness analysis (Fig. 3b), CSTP1 explained 39.0% of the variance, with the largest clusters spanning the insula, precentral gyrus and superior temporal gyrus. CSTP2 explained 9.8% of the variance, with the largest clusters spanning the insula, lingual gyrus, lateral occipital lobe, pericalcarine gyrus, parahippocampal gyrus and fusiform gyrus (Supplementary Table 4). All other CSTPs explained less than 10% of the variance and were excluded from further analyses. GAMs revealed

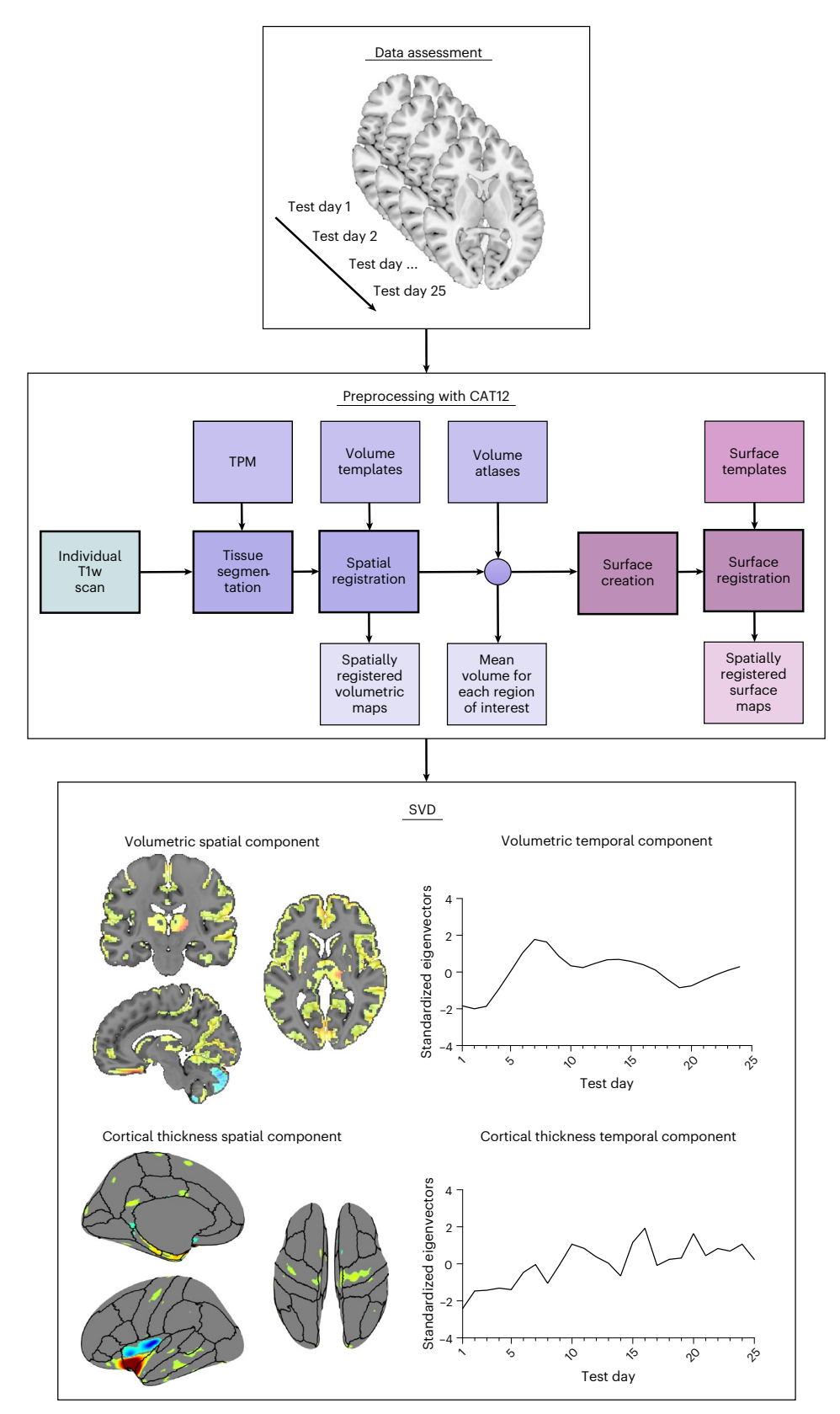
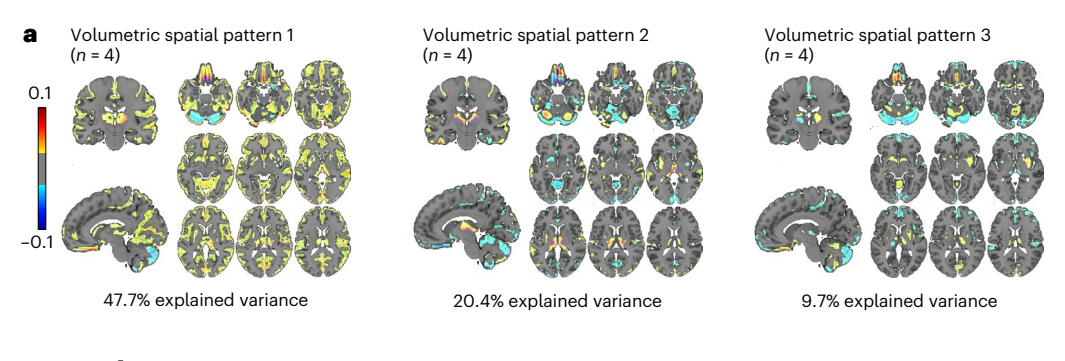


Fig. 2 | **Schematic illustration of data assessment, processing workflow and data reduction.** T1w images were assessed over a 4–5-week period for each participant. Images were then preprocessed using the longitudinal pipeline approach in CAT12. Next, SVD was applied to decompose the preprocessed images into spatial and temporal components. Spatial components represent changes in brain volumes and cortical thickness across different regions, while temporal components reflect how these spatial components evolve over time.

Warm and cool colors in the spatial component represent positive (warm colors) and negative (cool colors) associations between spatial components and temporal patterns. This suggests that regions marked in warm colors increase as the associated temporal pattern increases, while those in cool colors decrease. Note that the spatial and temporal components shown are examples and do not represent actual results. Graphs were created with GraphPad Prism (version 10). SVD, singular value decomposition; TPM, tissue probability maps.



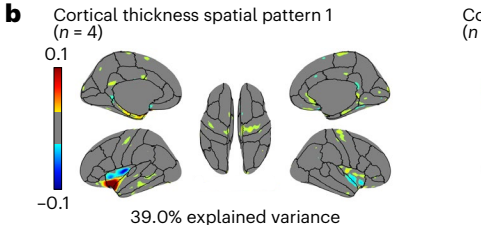
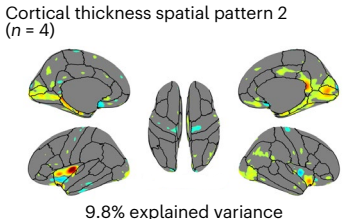


Fig. 3 | Volumetric and cortical thickness spatial patterns that explained at least 10% of the variance across the female participants (n=4). a, The spatial patterns illustrate the volumetric patterns of involved brain regions that change over time across the female participants (n=4; the endometriosis, oral contraceptives (OC), typical and 28andMe (typical) cycle). b, The spatial patterns illustrate the cortical thickness patterns of involved brain regions that change



over time across the female participants (n = 4; the endometriosis, OC, typical and 28 and Me (typical) cycle). For $\bf a$ and $\bf b$, volumetric and cortical thickness spatial patterns were derived using SVD. Spatial weights were thresholded, retaining only values within the ranges of -0.1 to -0.01 and 0.01 to 0.1, while excluding values between -0.01 and 0.01 that indicate minimal contribution to the respective spatial pattern (color bar).

that CSTP2 exhibited substantial fluctuations only in the 28 and Me (typical) cycle (Supplementary Table 5), and no significant fluctuations were observed in CSTP1 in any participant.

Hormonal associations with cortical thickness dynamics. Progesterone levels and the estradiol-to-progesterone ratio were significantly associated with CSPT2 in the 28andMe (typical) cycle only (progesterone, β = 0.042, $P_{\rm FDR}$ < 0.001; estradiol-to-progesterone ratio, β = 0.023, $P_{\rm FDR}$ < 0.001), supported by corresponding Spearman correlations (progesterone, ρ = 0.593, $P_{\rm FDR}$ = 0.002; estradiol-to-progesterone ratio, ρ = 0.612, $P_{\rm FDR}$ = 0.002). No significant associations were observed between other predictors and CSTP1 or CSTP2 in any of the remaining cycles. All results are displayed in Fig. 5 and Supplementary Table 6.

Complementary voxel-wise and vertex-wise analyses

To directly link hormonal fluctuations to structural brain measures, complementary voxel-wise and vertex-wise analyses were conducted as a sensitivity check. To confirm the hormone–SVD associations, we repeated the analyses at the voxel level (for volume) and the vertex level (for thickness) to assess whether similar spatial patterns of associations emerged.

Voxel-wise analyses revealed widespread positive associations between brain volume and hormonal concentrations of estradiol, progesterone and the estradiol-to-progesterone ratio across all individuals (Fig. 6a). These associations overlapped to some extent with the spatial patterns observed in the SVD analyses. Contrasted analyses indicated that the endometriosis and OC cycles predominantly drove the associations with estradiol levels, while associations with progesterone levels were primarily influenced by the typical and 28 and Me (typical) cycles (Fig. 6b). Estradiol levels were mainly positively associated with the cingulate gyrus, frontal gyrus, orbital gyrus, precentral gyrus, superior temporal gyrus and supramarginal gyrus. Progesterone levels and the estradiol-to-progesterone ratio were positively associated with the cerebellum, cuneus, inferior temporal, postcentral and superior parietal gyrus. Regions that were positively associated with both estradiol levels and progesterone levels, as well as the estradiol-to-progesterone

ratio, were the precuneus and angular gyrus (Supplementary Table 7). Negative associations were primarily observed in the OC cycle for the estradiol-to-progesterone ratio (Supplementary Table 8).

Vertex-wise analyses revealed only a few associations between cortical thickness and hormone concentrations. Significant positive associations were observed between the estradiol-to-progesterone ratio and cortical thickness of the parahippocampal and lateral occipital gyrus across all individuals (Fig. 7a). No significant associations were found with estradiol and progesterone levels. Contrasted analyses revealed significant positive associations between estradiol levels and cortical thickness of the postcentral, superior parietal, precentral and superior frontal gyrus in the endometriosis cycle only. The estradiol-to-progesterone ratio was associated with cortical thickness of the parahippocampal, lingual, lateral occipital, pericalcarine gyrus and cuneus only in the 28andMe (typical) cycle (Fig. 7b). No other significant associations were observed (Supplementary Table 9).

Comparison to a male participant

We repeated all analyses in a male participant where no specific gonadal hormone patterns were expected. The male participant was scanned over a comparable 5-week period, resulting in 25 test sessions (Extended Data Fig. 2a). Hormone concentrations were generally low (estradiol-M=128.7 pmol I^{-1} , s.d. = 17.3 pmol I^{-1} , range = 98.0–161.0 pmol I^{-1} ; progesterone-M=0.863 nmol I^{-1} , s.d. = 0.582 nmol I^{-1} , range = 0.329–3.420 nmol I^{-1} ; ratio-M=6.921, s.d. = 5.049, range = 2.35–28.74; Extended Data Fig. 2b).

VSTP analyses revealed that VSTP1 explained 58.0% of the variance, VSTP2 explained 19.3% of the variance and VSTP3 explained 12.9% of the variance (Extended Data Fig. 3). CSTP analyses revealed that CSTP1 explained 40.2% of the variance, CSTP2 explained 14.2% of the variance and CSTP3 explained 11.3% of the variance (Extended Data Fig. 4). All other volumetric and CSTPs explained less than 10% of the variance and were excluded from further analyses.

While VSTP1-VSTP3 significantly changed across the 5-week period (Supplementary Table 10), no associations were found with either estradiol levels, progesterone levels or the estradiol-to-progesterone

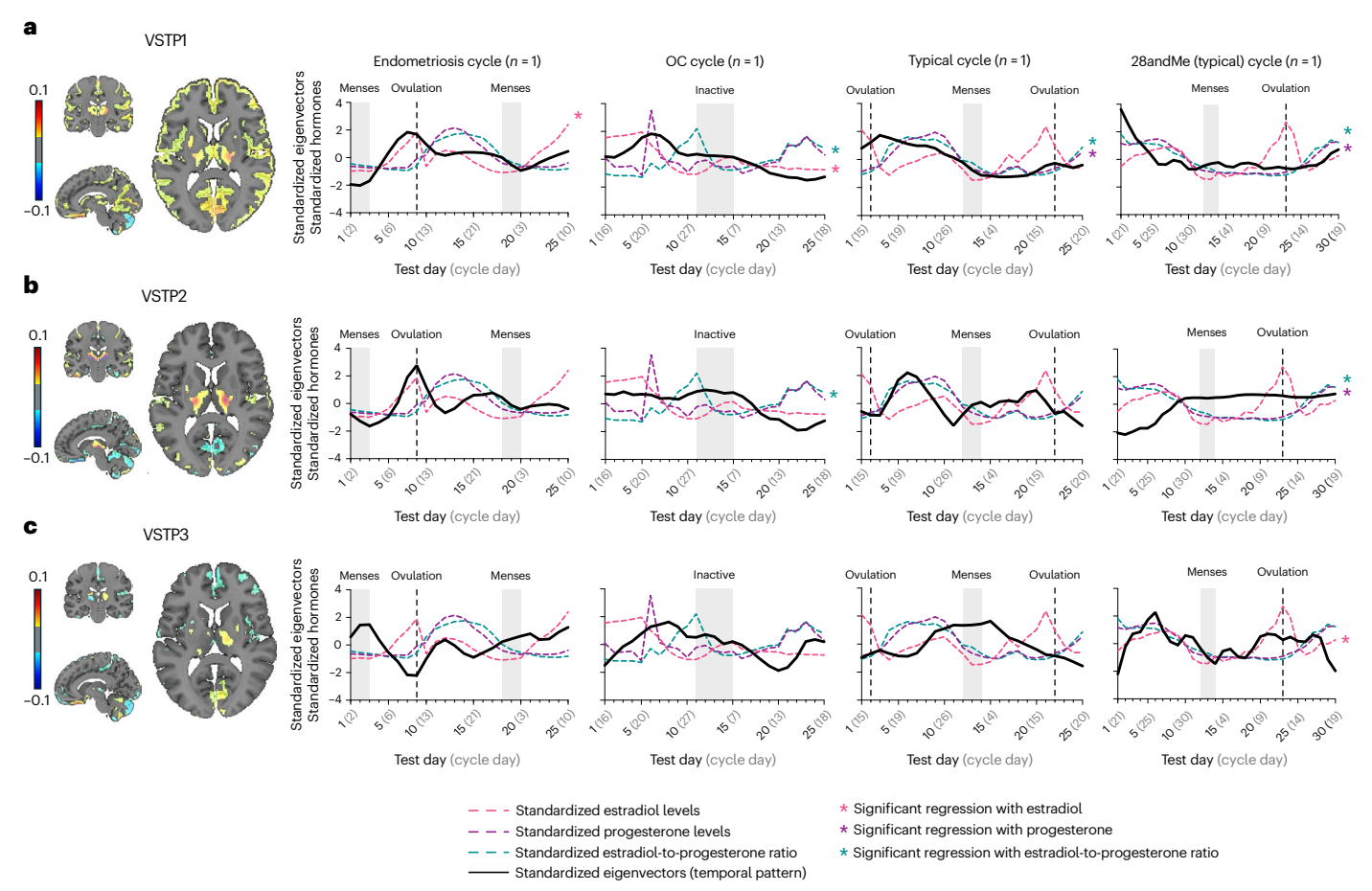


Fig. 4 | VSTPs across the different female cycles (n = 4). This figure depicts VSTPs across the endometriosis cycle, the oral contraceptives (OC) cycle, the typical cycle and the 28andMe (typical) cycle. a. VSTP1 shows spatial distribution of brain regions involved in component 1 (left) and the associated temporal dynamics (right). Warm colors in the spatial map indicate regions with positive associations to the temporal pattern (indicating regional volume increases as the temporal pattern increases). Cool colors in the spatial map indicate negative associations to the temporal pattern (reflecting regional volume decreases as the temporal pattern increases). **b**, VSTP2 shows spatial distribution of brain regions involved in component 2 (left) and the associated temporal dynamics (right). Warm colors in the spatial map indicate regions with positive associations to the temporal pattern (indicating regional volume increases as the temporal pattern increases). Cool colors in the spatial map indicate negative associations to the temporal pattern (reflecting regional volume decreases as the temporal pattern increases). c, VSTP3 shows spatial distribution of brain regions involved in component 3 (left) and the associated temporal dynamics (right). Warm colors

in the spatial map indicate regions with positive associations to the temporal pattern (indicating regional volume increases as the temporal pattern increases). Cool colors in the spatial map indicate negative associations to the temporal pattern (reflecting regional volume decreases as the temporal pattern increases). For a-c, volumetric and cortical thickness spatial patterns were derived using SVD. Spatial weights were thresholded, retaining only values within the ranges of -0.1 to -0.01 and 0.01 to 0.1, while excluding values between -0.01 and 0.01 that indicate minimal contribution to the respective spatial pattern (color bar). Solid black lines represent standardized eigenvectors (temporal pattern); dashed colored lines represent square-rooted and standardized hormonal values; gray shading indicates menses in typical cycles and the endometriosis cycle, and inactive pill phase in the OC cycle; dotted lines indicate ovulation. Asterisks indicate significant time-series regressions between hormone levels and the spatiotemporal patterns after FDR correction for multiple comparisons was performed. For exact P values, see main text. Plots were created with GraphPad Prism (version 10). VSTPs, volumetric spatiotemporal patterns.

ratio (Supplementary Table 11). CSTP1–CSTP3 did not show significant changes across the 5-week period and were not associated with hormone concentrations (Supplementary Tables 10-11). Likewise, the voxel-wise and vertex-wise analyses revealed no significant associations with hormone concentrations (Extended Data Fig. 5).

Discussion

Despite growing interest in the associations between gonadal hormones and fluctuations in brain structure, whole-brain approaches with broader spatiotemporal resolution are scarce. Such analyses provide insights into how the brain operates synchronously over time. Moreover, investigations into hormone-brain interactions in nontypical cycles—such as those in endometriosis or hormonal contraceptive use—remain understudied. In the present study, we leveraged data from four densely sampled females—two with typical cycles, one

with endometriosis and one using OC—and one male, each of whom underwent routine neuroimaging and venipuncture over a monthly period. Using a whole-brain SVD analytical approach, we explored brain structural dynamics across these diverse hormonal conditions. The corresponding datasets are openly available, providing a resource for future investigations into brain plasticity across menstrual cycles and beyond.

While previous precision imaging studies have focused on region-specific analyses 40,41, here we extend this work by examining whole-brain structural dynamics across the menstrual cycle. Results revealed VSTPs that exhibited substantial variations in all four female individuals across the monthly period. These fluctuations were widespread and distributed across the entire brain. Notably, while these patterns were observed in all four female individuals, the nature and dynamics of how these widespread patterns fluctuated over the

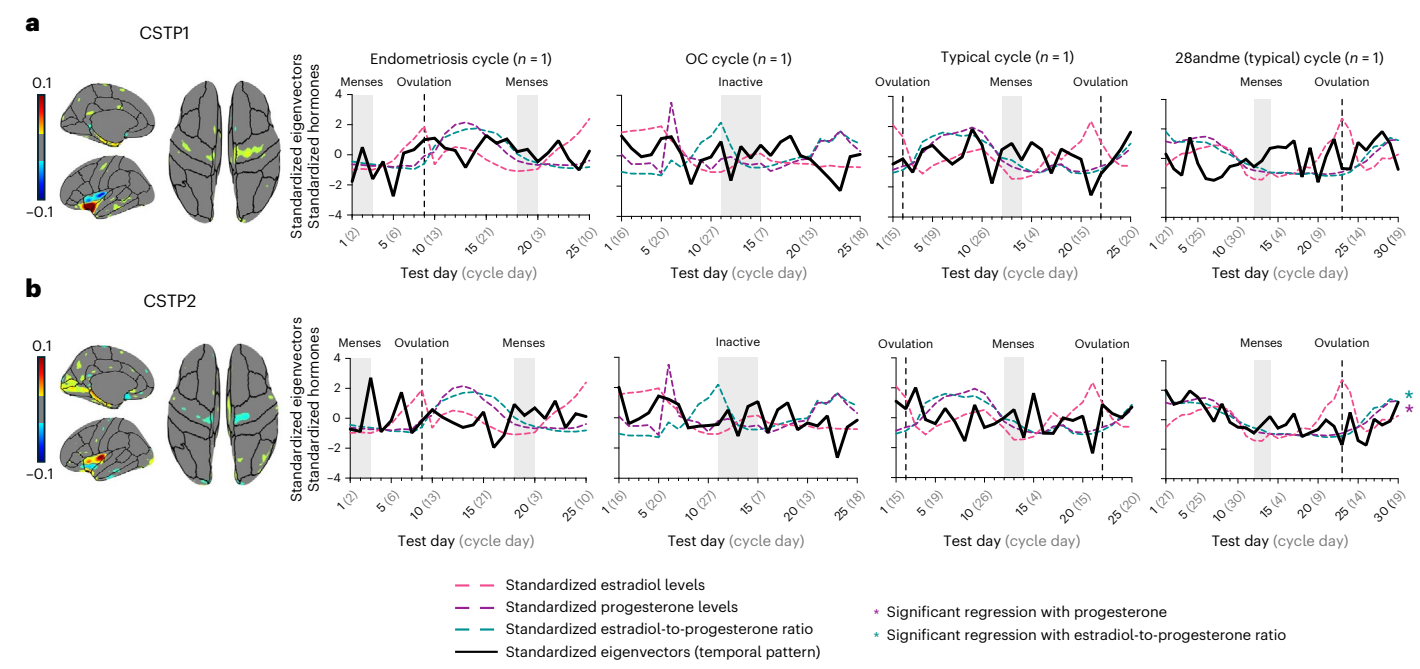


Fig. 5 | **CSTPs across the different female cycles** (n = 4). This figure depicts CSTPs across the endometriosis cycle, the OC cycle, the typical cycle and the 28andMe (typical) cycle. **a**, CSTP1 shows spatial distribution of brain regions involved in component 1 (left) and the associated temporal dynamics (right). Warm colors in the spatial map indicate regions with positive associations to the temporal pattern (indicating regional cortical thickness increases as the temporal pattern increases). Cool colors in the spatial map indicate negative associations to the temporal pattern (reflecting regional cortical thickness decreases as the temporal pattern increases). **b**, CSTP2 shows spatial distribution of brain regions involved in component 2 (left) and the associated temporal dynamics (right). Warm colors in the spatial map indicate regions with positive associations to the temporal pattern (indicating regional cortical thickness increases as the temporal pattern increases). Cool colors in the spatial map indicate negative associations to the temporal pattern (reflecting regional

cortical thickness decreases as the temporal pattern increases). For $\bf a$ and $\bf b$, volumetric and cortical thickness spatial patterns were derived using SVD. Spatial weights were thresholded, retaining only values within the ranges of -0.1 to -0.01 and 0.01 to 0.1, while excluding values between -0.01 and 0.01 that indicate minimal contribution to the respective spatial pattern (color bar). Solid black lines represent standardized eigenvectors (temporal pattern); dashed colored lines represent square-rooted and standardized hormonal values; gray shading indicates menses in typical cycles and the endometriosis cycle, and inactive pill phase in the OC cycle; dotted lines indicate ovulation. Asterisks indicate significant time-series regressions between hormone levels and the spatiotemporal patterns after FDR correction for multiple comparisons was performed. For exact P values, see main text. Plots were created with GraphPad Prism (version 10). CSTPs, cortical thickness spatiotemporal patterns.

monthly period were unique to each individual. Interestingly, the temporal dynamics of the volumetric spatial pattern explaining the most variance were most similar in the endometriosis and OC cycle, which are both characterized by a hormonal milieu dominated by estradiol. In contrast, individuals with typical cycles exhibited more similar temporal dynamics of the volumetric spatial pattern, which explained the most variance, reflecting the cyclical interplay between progesterone and estradiol. Notably, the hormonal correlates of this dominant pattern differed by cycle type—estradiol in the endometriosis and OC cycle, and progesterone in the typical cycles. The association of this pattern with gonadal hormones across all cycles supports the notion that while hormones do have a role in shaping cyclical brain dynamics, not all structural variation across the cycle is hormone-driven and acknowledges the multidimensional nature of brain plasticity.

CSTPs, however, did not fluctuate across individuals, with the exception of the 28andMe (typical) cycle. Cortical thickness analyses inherently exclude the cerebellum and subcortical structures, which have been shown to substantially contribute to the whole-brain SVD patterns observed in volumetric analyses. The cerebellum, as well as subcortical structures, are known to contain sex steroid receptors^{4,5}, which may make them particularly sensitive to hormonal fluctuations. The exclusion of these structures in cortical thickness analyses may partly explain why, at the whole-brain level, CSTPs did not exhibit fluctuations across the cycle or show associations with sex steroid hormones. Another explanation for the absence of fluctuations and associations in the cortical thickness measures may lie in the underlying

biophysical properties that drive both volumetric and cortical thickness signals. For example, the presence of greater changes observable in gray matter volume could reflect a contribution of changes in water content across the menstrual cycle rather than changes in neuronal and glial structures within the gray matter. While volumetric and cortical thickness estimates are both derived from T1w magnetic resonance imaging (MRI) data, water content variations are more likely to affect volumetric measures due to shifts in extracellular fluid dynamics, which may be influenced by hormonal changes 56-58, than cortical thickness measures, which are less sensitive to such transient changes 59.

Preclinical literature indicates that progesterone exerts an inhibitory effect on proliferative actions of estradiol⁵. For example, animal studies have shown that estradiol enhances the excitability of fast-spiking interneurons in deep cortical layers 60 and increases synapse formation in the prefrontal cortex8. However, concurrent cyclic administration of progesterone attenuates this increase in spine density when paired with estradiol⁶¹. Additionally, progesterone exhibits a similar inhibitory effect on dendritic spines in the hippocampus¹⁰. In line with these findings, our study suggests that individuals with typical menstrual cycles exhibit a heightened sensitivity to progesterone. We observed fluctuations in brain volumes over the monthly period in both typical cycles and in the case of hormonal dysregulation, with progesterone exerting a more pronounced influence on structural brain dynamics in typical cycles. These findings are consistent with previous research using the 28andMe dataset, revealing substantial associations between progesterone and the medial temporal lobe.

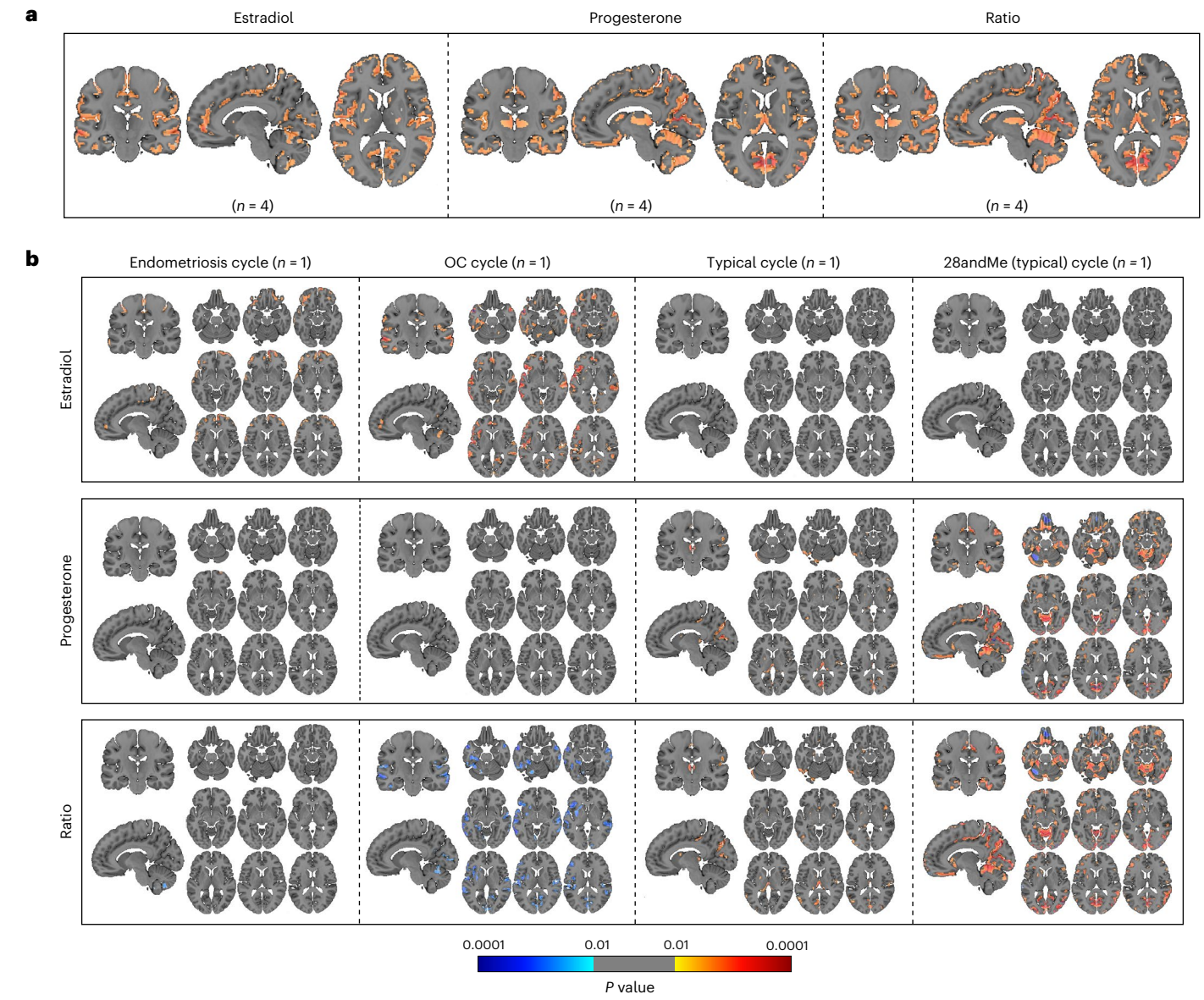


Fig. 6 | **Significant voxels associated with hormone concentrations in the female participants** (n = 4). **a**, The significant voxel-wise associations across all four cycles (n = 4; endometriosis cycle, oral contraceptives (OC) cycle, typical cycle and 28andMe (typical) cycle). **b**, The presentation of the significant voxels for each cycle separately (endometriosis cycle, n = 1; OC cycle, n = 1; typical cycle, n = 1; and 28andMe (typical) cycle, n = 1). For **a** and **b**, GLMs were used for vertex-

wise analysis with the TFCE method that controls for multiple comparisons by applying an FWE correction. Hormone concentrations were square-rooted. Positive associations are displayed in red, negative associations are displayed in blue, with P values ranging from 0.01 to 0.0001 (color bar). GLMs, general linear models; TFCE, threshold-free cluster enhancement; FWE, family-wise error; Ratio, estradiol-to-progesterone ratio.

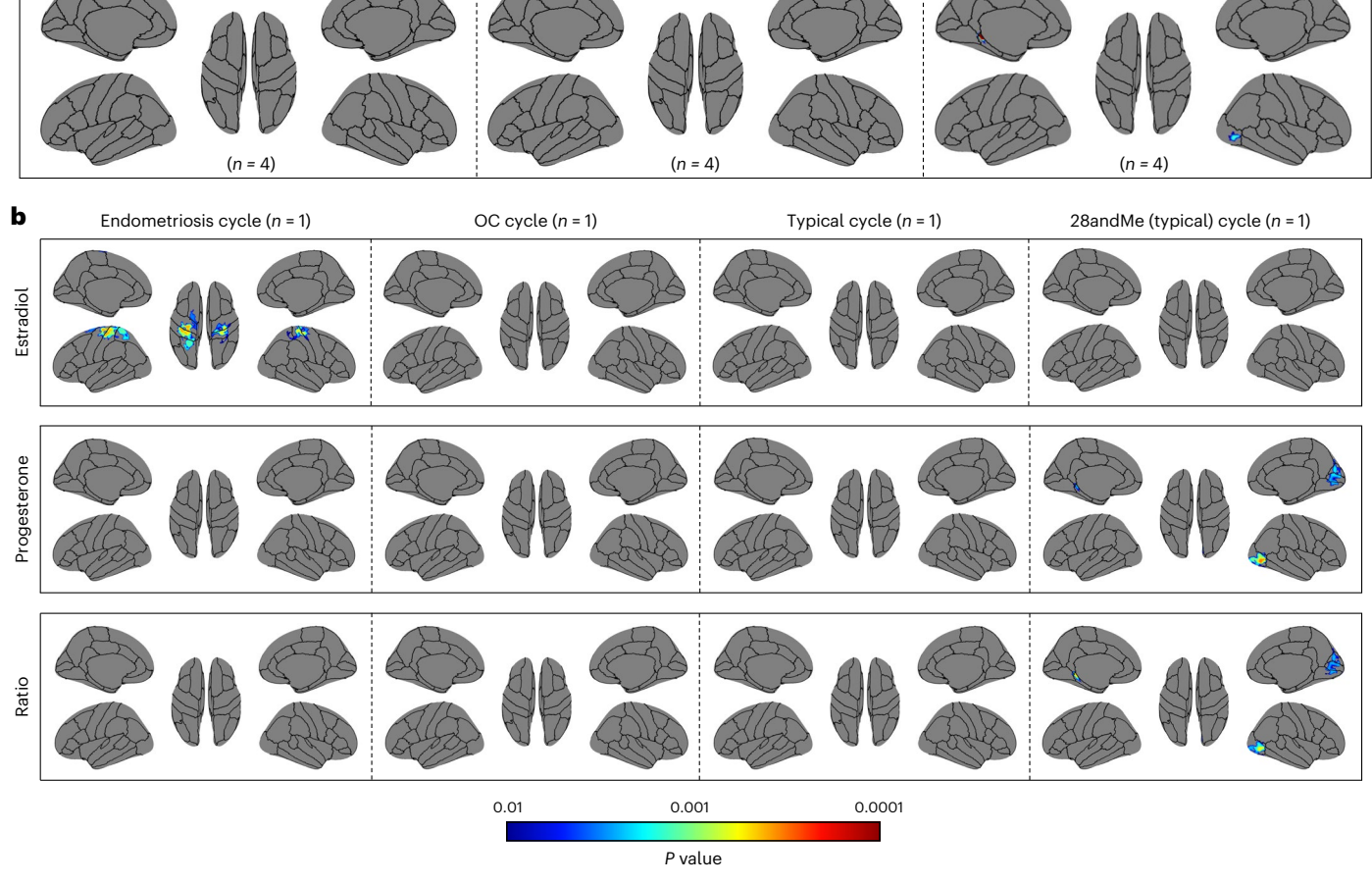
These associations were abolished when progesterone was selectively suppressed and estradiol dominated 40. In contrast, when estradiol is the dominating hormone throughout the cycle, as observed in endometriosis, it appears to exert a greater impact on structural brain dynamics, potentially exerting its proliferative actions. Our findings align with previous literature 48-50,52, indicating elevated estradiol levels and estradiol dominance in the luteal phase of the menstrual cycle in endometriosis, suggesting a greater exposure of estradiol on the brain. Additionally, our results in the female using OC, providing an additional dataset with a hormonal milieu similar to the endometriosis cycle, further underscore the influence of estradiol dominance on brain structure. Voxel-wise analyses further supported these associations. While implicated regions varied between individuals, the most consistent finding, across both voxel-wise and SVD analyses, was that progesterone was the primary correlate of brain volume changes in

the typical cycles, whereas estradiol was the primary correlate in the endometriosis and OC cycle.

Estrogen is believed to have a neuroprotective role, promoting brain health and protecting against cognitive decline 62-64. However, while estradiol levels within the physiological range stimulate brain activity, especially in the hippocampus, supraphysiological levels of estradiol (equivalent to those during early pregnancy) exhibit opposite effects 65. Interestingly, unopposed estrogen during hormone replacement therapy in menopause enhances activation of fronto-cingulate regions during cognitive functioning tasks 66. This highlights the specific impact of elevated estrogen levels, unbalanced by other hormones, on brain activity and cognition. Little is known about the impact of prolonged high estradiol exposure during the reproductive years on long-term health outcomes. This underscores the importance of further research to elucidate the longitudinal relationships among

Estradiol

Ratio



Progesterone

Fig. 7 | Significant vertices associated with hormone concentrations in the female participants (n=4). a, The significant vertex-wise associations across all four cycles (n=4; endometriosis cycle, oral contraceptives (OC) cycle, typical cycle and 28andMe (typical) cycle). b, The presentation of the significant vertices for each cycle separately (endometriosis cycle, n=1; OC cycle, n=1; typical cycle,

n=1; and 28andMe (typical) cycle, n=1). For **a** and **b**, GLMs were used for vertexwise analysis with the TFCE method that controls for multiple comparisons by applying an FWE correction. Hormone concentrations were square-rooted. Only positive associations were observed, with P values ranging from 0.01 to 0.0001 (color bar). Ratio, estradiol-to-progesterone ratio.

gonadal hormones, reproductive health and long-term well-being in individuals with hormonal dysregulations.

To further contextualize our findings, we expanded the scope of our study by including additional analyses of one male over a densely sampled 5-week period. While VSTPs fluctuated over the 5-week period, these changes were not associated with hormone concentrations. This is not surprising given that the substantially reduced magnitude of hormonal fluctuations in the male participant compared to what is observed and characteristic of a menstrual cycle. It also suggests that the observed spatiotemporal fluctuations may not be detectably driven by those hormones but could be influenced by factors not accounted for in this investigation, such as intake of water, or cerebral blood flow. Furthermore, these results may indicate the presence of different regulatory mechanisms or hormonal thresholds in males compared to females. However, this requires further investigation in future studies that explore diurnal changes or manipulate hormones in males. Such studies can provide clearer insights into sex and sex-hormone differences as most recently demonstrated⁶⁷. Furthermore, the absence of substantial hormone-brain associations in the male participant suggests that the associations observed in female participants are likely driven by cyclical variations in gonadal hormones rather than general intersession variability and underscores the importance of studying female-specific endocrinological influences on brain structure. This area of research has historically been underrepresented in the field of neuroscience.

The study has several limitations. First, because these are dense-sampling datasets with a limited sample size, caution is advised when generalizing the findings to the broader population. By focusing on individual participants, we aimed to mitigate the intra-individual variability of hormonal and brain structural fluctuations, thereby providing clearer insight into personalized spatiotemporal patterns that are often obscured in studies with larger samples. Our approach provides a more precise examination of the specific patterns of brain structure and hormonal fluctuations at an individual level, offering a higher level of sensitivity and temporal resolution toward precision imaging. Second, this study applied a model-free whole-brain approach. Using SVD represents a new method for exploring short-term structural brain changes across the menstrual cycle. This approach helps to identify unique spatiotemporal profiles, thereby potentially mechanistic principles underlying structural brain changes throughout the menstrual cycle. The data-driven nature of our approach contrasts with the more common hypothesis-driven studies that focus on predefined regions of interest. While our model-free strategy allows for the discovery of hormone-brain associations in less commonly studied areas, it did not identify particular regions consistently across individuals to target in future research. Instead, it highlights that the entire brain undergoes

individual structural changes across menstrual cycles, changes that are partly driven by gonadal hormones. However, all imaging data used in these analyses will be made openly available upon publication, allowing for targeted follow-up analyses using regions of interest or established network templates. Third, we identified unique temporal patterns in each participant, precluding direct comparisons between them. Moreover, variations in sampling strategies were observed among participants. While the 28 and Me (typical) cycle was sampled daily for four consecutive weeks, scanning in the typical, the endometriosis and the OC cycle occurred primarily on weekdays for five consecutive weeks. For instance, the longest scanning gap in the typical cycle spanned 4 days. These differences might explain why weaker associations were observed in the typical cycle and stronger associations in the 28 and Me (typical) cycle. Variations in scanning schedules and differences in participants' age and factors such as nicotine use in one participant may contribute to divergent temporal patterns that should not be directly compared. For instance, nicotine acutely inhibits aromatase in the thalamus in healthy females, thereby it blocks the local synthesis of estrogen from androgen precursors⁶⁸. Notably, the finding that estradiol levels were associated with brain volume in estradiol-dominant cycles and progesterone levels in progesterone-dominant cycles was more consistent than the specific regions implicated, suggesting robust yet individualized brain-hormone coupling. These results underscore the need to focus on personalized spatiotemporal patterns in both brain structure and hormonal levels. Menstrual cycle dynamics and other intra-individual factors that influence our measures of interest are inherently variable within-person⁶⁹. Thus, while there is some consistency across individuals and cycles in the dominant spatiotemporal pattern and the voxel-wise analysis (precision), hormone-brain associations remain noisy and difficult to replicate across individuals. Fourth, our study revealed dynamic brain changes not only in females but also in a male participant. In females, these changes were associated with fluctuations in estradiol and progesterone levels, but the mechanisms driving similar changes in males remain unclear. Finally, we compared gonadal hormone levels among the four participants, but different steroid analyses were used in the typical, the endometriosis and the OC cycle compared to the 28 and Me (typical) cycle. Hormones were identified through immunoassay (IAs) in the typical, endometriosis and the OC cycle, while, in the 28andMe (typical) cycle, hormones were identified through liquid chromatography-mass spectrometry (LC-MS). While IAs offer a higher sample turnover, they are limited in trueness. precision and sensitivity. In contrast, LC-MS has been demonstrated to deliver better sensitivity and specificity. However, good overall method agreement was found for estradiol and progesterone^{70,71}. Future studies should consider using consistent steroid analyses to ensure comparability, or harmonization methods should be developed to enable the integration of hormone assessments, allowing the pooling of data from multiple research sites to increase power, reproducibility and generalizability⁷².

Further research using whole-brain approaches and spatiotemporal patterns with larger and more diverse samples is necessary to validate and expand these initial findings. Future research should address potential interindividual variations and strive to enhance the generalizability of the observed associations. Despite the small sample size, our findings provide valuable initial insights into the dynamic impact of hormonal fluctuations on whole-brain structural plasticity throughout the menstrual cycle and under conditions of nontypical hormonal regulation. While specific regional changes were not the focus of this study, the consistent spatial maps and unique temporal patterns emphasize a widespread, coordinated influence of hormonal changes on brain structure. From a translational perspective, our findings hold important implications for the interpretation of animal studies on hormone-brain interactions. While animal models provide valuable insights into cellular and molecular mechanisms, our results emphasize that hormone-driven volumetric changes in humans

are not confined to limbic structures, such as the hippocampus, but extend to widespread cortical and cerebellar regions. Future studies should aim to integrate methodologies that allow for cross-species comparisons, ensuring that findings from animal models align with the distributed brain networks implicated in human neuroendocrine dynamics. Furthermore, animal models of hormone–brain interactions often focus on acute manipulations of estradiol or progesterone. Yet, our data emphasize the importance of naturally occurring hormone fluctuations and their interaction over time. Given the distinct patterns observed in cycles with estradiol dominance versus typical cycles, future animal studies should consider the broader hormonal milieu rather than focusing on individual hormones in isolation.

In summary, our study lays the groundwork for a future in personalized and precision medicine, offering initial insights into how distinct hormonal milieus—such as the interplay between estradiol and progesterone levels in typical cycles or estradiol dominance in endometriosis—affect brain structure. Rather than identifying brain regions universally linked to specific hormones, our results underscore that hormone—brain associations vary across individuals and are milieu-dependent. These associations appear to be influenced by the presence or the absence of natural hormonal fluctuations, emphasizing the importance of within-person designs to capture the dynamic nature of hormone-related brain plasticity.

Online content

Any methods, additional references, Nature Portfolio reporting summaries, source data, extended data, supplementary information, acknowledgements, peer review information; details of author contributions and competing interests; and statements of data and code availability are available at https://doi.org/10.1038/s41593-025-02066-2.

References

- Fehring, R. J., Schneider, M. & Raviele, K. Variability in the phases of the menstrual cycle. J. Obstet. Gynecol. Neonatal Nurs. 35, 376–384 (2006).
- Roos, J. et al. Monitoring the menstrual cycle: comparison of urinary and serum reproductive hormones referenced to true ovulation. Eur. J. Contracept. Reprod. Health Care 20, 438–450 (2015).
- Abraham, G. E., Odell, W. D., Swerdloff, R. S. & Hopper, K. Simultaneous radioimmunoassay of plasma FSH, LH, progesterone, 17-hydroxyprogesterone, and estradiol-17β during the menstrual cycle. J. Clin. Endocrinol. Metab. 34, 312–318 (1972).
- Österlund, M. K., Gustafsson, J. Å., Keller, E. & Hurd, Y. L. Estrogen receptor β (ERβ) messenger ribonucleic acid (mRNA) expression within the human forebrain: distinct distribution pattern to ERα mRNA. J. Clin. Endocrinol. Metab. 85, 3840–3846 (2000).
- 5. Brinton, R. D. et al. Progesterone receptors: form and function in brain. *Front. Neuroendocrinol.* **29**, 313 (2008).
- Woolley, C. S., Gould, E., Frankfurt, M. & McEwen, B. S. Naturally occurring fluctuation in dendritic spine density on adult hippocampal pyramidal neurons. *J. Neurosci.* 10, 4035–4039 (1990).
- Haraguchi, S. et al. Estradiol promotes Purkinje dendritic growth, spinogenesis, and synaptogenesis during neonatal life by inducing the expression of BDNF. Cerebellum 11, 416–417 (2012).
- 8. Hara, Y., Waters, E. M., McEwen, B. S. & Morrison, J. H. Estrogen effects on cognitive and synaptic health over the lifecourse. *Physiol. Rev.* **95**, 785–807 (2015).
- Tsutsui, K. Progesterone biosynthesis and action in the developing neuron. Endocrinology 149, 2757–2761 (2008).
- Woolley, C. S. & McEwen, B. S. Roles of estradiol and progesterone in regulation of hippocampal dendritic spine density during the estrous cycle in the rat. J. Comp. Neurol. 336, 293–306 (1993).

- Galea, L. A. M., Frick, K. M., Hampson, E., Sohrabji, F. & Choleris, E. Why estrogens matter for behavior and brain health. *Neurosci*. *Biobehav. Rev.* 76, 363–379 (2017).
- Juraska, J. M., Sisk, C. L. & DonCarlos, L. L. Sexual differentiation of the adolescent rodent brain: hormonal influences and developmental mechanisms. Horm. Behav. 64, 203–210 (2013).
- Rehbein, E., Hornung, J., Sundström Poromaa, I. & Derntl, B. Shaping of the female human brain by sex hormones: a review. Neuroendocrinology 111, 183–206 (2021).
- Dubol, M. et al. Neuroimaging the menstrual cycle: a multimodal systematic review. Front. Neuroendocrinol. 60, 100878 (2021).
- Jacobs, E. & D'Esposito, M. Estrogen shapes dopamine-dependent cognitive processes: implications for women's health. *J. Neurosci.* 31, 5286–5293 (2011).
- Kim, J. & Frick, K. M. Distinct effects of estrogen receptor antagonism on object recognition and spatial memory consolidation in ovariectomized mice. *Psychoneuroendocrinology* 85, 110–114 (2017).
- Frick, K. M., Kim, J., Tuscher, J. J. & Fortress, A. M. Sex steroid hormones matter for learning and memory: estrogenic regulation of hippocampal function in male and female rodents. *Learn. Mem.* 22, 472–493 (2015).
- Berman, K. F. et al. Modulation of cognition-specific cortical activity by gonadal steroids: a positron-emission tomography study in women. Proc. Natl Acad. Sci. USA 94, 8836–8841 (1997).
- Oyola, M. G. & Handa, R. J. Hypothalamic-pituitary-adrenal and hypothalamic-pituitary-gonadal axes: sex differences in regulation of stress responsivity. Stress 20, 476-494 (2017).
- Heck, A. L. & Handa, R. J. Sex differences in the hypothalamicpituitary-adrenal axis' response to stress: an important role for gonadal hormones. Neuropsychopharmacology 44, 45–58 (2018).
- Jacobs, E. G. et al. 17β-estradiol differentially regulates stress circuitry activity in healthy and depressed women. Neuropsychopharmacology 40, 566–576 (2014).
- Andersen, E. et al. Methods for characterizing ovarian and adrenal hormone variability and mood relationships in peripubertal females. Psychoneuroendocrinology 141, 105747 (2022).
- Gordon, J. L., Sander, B., Eisenlohr-Moul, T. A. & Sykes Tottenham, L. Mood sensitivity to estradiol predicts depressive symptoms in the menopause transition. *Psychol. Med.* 51, 1733–1741 (2021).
- Münster, K., Schmidt, L. & Helm, P. Length and variation in the menstrual cycle—a cross-sectional study from a Danish county. Br. J. Obstet. Gynaecol. 99, 422–429 (1992).
- Dubol, M., Epperson, C. N., Lanzenberger, R., Sundström-Poromaa, I. & Comasco, E. Neuroimaging premenstrual dysphoric disorder: a systematic and critical review. Front. Neuroendocrinol. 57, 100838 (2020).
- Hagemann, G. et al. Changes in brain size during the menstrual cycle. PLoS ONE 6, e14655 (2011).
- Pletzer, B., Harris, T. & Hidalgo-Lopez, E. Subcortical structural changes along the menstrual cycle: beyond the hippocampus. Sci. Rep. 8, 16042 (2018).
- Lisofsky, N. et al. Hippocampal volume and functional connectivity changes during the female menstrual cycle. *Neuroimage* 118, 154–162 (2015).
- 29. Pletzer, B. et al. Menstrual cycle and hormonal contraceptive use modulate human brain structure. *Brain Res.* **1348**, 55–62 (2010).
- De Bondt, T. et al. Regional gray matter volume differences and sex-hormone correlations as a function of menstrual cycle phase and hormonal contraceptives use. *Brain Res.* 1530, 22–31 (2013).
- 31. Poldrack, R. A. et al. Long-term neural and physiological phenotyping of a single human. *Nat. Commun.* **6**, 8885 (2015).
- Gordon, E. M. et al. Precision functional mapping of individual human brains. Neuron 95, 791–807 (2017).

- 33. Greenwell, S. et al. High-amplitude network co-fluctuations linked to variation in hormone concentrations over the menstrual cycle. *Netw. Neurosci.* **7**, 1181–1205 (2023).
- 34. Pritschet, L., Taylor, C. M., Santander, T. & Jacobs, E. G. Applying dense-sampling methods to reveal dynamic endocrine modulation of the nervous system. *Curr. Opin. Behav. Sci.* **40**, 72–78 (2021).
- 35. De Filippi, E. et al. The menstrual cycle modulates whole-brain turbulent dynamics. *Front. Neurosci.* **15**, 753820 (2021).
- Mueller, J. M. et al. Dynamic community detection reveals transient reorganization of functional brain networks across a female menstrual cycle. *Netw. Neurosci.* 5, 125–144 (2021).
- Pritschet, L. et al. Functional reorganization of brain networks across the human menstrual cycle. *Neuroimage* 220, 117091 (2020).
- 38. Fitzgerald, M., Pritschet, L., Santander, T., Grafton, S. T. & Jacobs, E. G. Cerebellar network organization across the human menstrual cycle. *Sci. Rep.* **10**, 20732 (2020).
- 39. Barth, C. et al. In-vivo dynamics of the human hippocampus across the menstrual cycle. *Sci. Rep.* **6**, 32833 (2016).
- Taylor, C. M. et al. Progesterone shapes medial temporal lobe volume across the human menstrual cycle. *Neuroimage* 220, 117125 (2020).
- 41. Zsido, R. G. et al. Ultra-high-field 7T MRI reveals changes in human medial temporal lobe volume in female adults during menstrual cycle. *Nat. Ment. Health* 1, 761–771 (2023).
- 42. Vercellini, P., Viganò, P., Somigliana, E. & Fedele, L. Endometriosis: pathogenesis and treatment. *Nat. Rev. Endocrinol.* **10**, 261–275 (2014).
- 43. Zondervan, K. T. et al. Endometriosis. Nat. Rev. Dis. Prim. 4, 9 (2018).
- Burney, R. O. et al. Gene expression analysis of endometrium reveals progesterone resistance and candidate susceptibility genes in women with endometriosis. *Endocrinology* **148**, 3814– 3826 (2007).
- 45. Shafrir, A. L. et al. Risk for and consequences of endometriosis: a critical epidemiologic review. *Best Pract. Res. Clin. Obstet. Gynaecol.* **51**, 1–15 (2018).
- Giudice, L. C. & Kao, L. C. Endometriosis. Lancet 364, 1789–1799 (2004).
- Zondervan, K. T., Becker, C. M. & Missmer, S. A. Endometriosis. N. Engl. J. Med. 382, 56 (2020).
- 48. Zeitoun, K. M. & Bulun, S. E. Aromatase: a key molecule in the pathophysiology of endometriosis and a therapeutic target. *Fertil. Steril.* **72**, 961–969 (1999).
- Zeitoun, K., Takayama, K., Michael, M. D. & Bulun, S. E. Stimulation of aromatase P450 promoter (II) activity in endometriosis and its inhibition in endometrium are regulated by competitive binding of steroidogenic factor-1 and chicken ovalbumin upstream promoter transcription factor to the same cis-acting element. *Mol. Endocrinol.* 13, 239–253 (1999).
- Zeitoun, K. et al. Deficient 17β-hydroxysteroid dehydrogenase type 2 expression in endometriosis: failure to metabolize 17β-estradiol. J. Clin. Endocrinol. Metab. 83, 4474–4480 (1998).
- 51. Attia, G. R. et al. Progesterone receptor isoform A but not B is expressed in endometriosis. *J. Clin. Endocrinol. Metab.* **85**, 2897–2902 (2000).
- Lessey, B. A., Metzger, D. A., Haney, A. F. & McCarty, K. S. Immunohistochemical analysis of estrogen and progesterone receptors in endometriosis: comparison with normal endometrium during the menstrual cycle and the effect of medical therapy. Fertil. Steril. 51, 409–415 (1989).
- Bergqvist, A. & Fernö, M. Endometriosis: oestrogen and progesterone receptors in endometriotic tissue and endometrium: comparison of different cycle phases and ages. *Hum. Reprod.* 8, 2211–2217 (1993).

- 54. Leiva, R., Bouchard, T., Boehringer, H., Abulla, S. & Ecochard, R. Random serum progesterone threshold to confirm ovulation. *Steroids* **101**, 125–129 (2015).
- Gaser, C. et al. CAT: a computational anatomy toolbox for the analysis of structural MRI data. *GigaScience* https://doi.org/ 10.1093/gigascience/giaeO49 (2024).
- Wenner, M. M., Stachenfeld, N. S., Wenner, M. M. & Stachenfeld, N. S. Blood pressure and water regulation: understanding sex hormone effects within and between men and women. *J. Physiol.* 590, 5949–5961 (2012).
- Hampl, R., Bičíková, M. & Sosvorová, L. Hormones and the blood-brain barrier. Horm. Mol. Biol. Clin. Investig. 21, 159–164 (2015).
- 58. Stachenfeld, N. S. Sex hormone effects on body fluid regulation. Exerc. Sport Sci. Rev. **36**. 152–159 (2008).
- Streitbürger, D. P. et al. Investigating structural brain changes of dehydration using voxel-based morphometry. PLoS ONE 7, e44195 (2012).
- 60. Clemens, A. M. et al. Estrus-cycle regulation of cortical inhibition. *Curr. Biol.* **29**, 605–615 (2019).
- 61. Ohm, D. T. et al. Clinically relevant hormone treatments fail to induce spinogenesis in prefrontal cortex of aged female rhesus monkeys. *J. Neurosci.* **32**, 11700–11705 (2012).
- 62. Dubal, D. B. et al. Estrogen receptor α , not β , is a critical link in estradiol-mediated protection against brain injury. *Proc. Natl Acad. Sci. USA* **98**, 1952–1957 (2001).
- 63. Roof, R. L. & Hall, E. D. Gender differences in acute CNS trauma and stroke: neuroprotective effects of estrogen and progesterone. *J. Neurotrauma* **17**, 367–388 (2000).
- 64. Luine, V. N. Estradiol and cognitive function: past, present and future. *Horm. Behav.* **66**, 602–618 (2014).
- Bayer, J., Gläscher, J., Finsterbusch, J., Schulte, L. H. & Sommer, T. Linear and inverted U-shaped dose-response functions describe estrogen effects on hippocampal activity in young women. *Nat.* Commun. 9, 1220 (2018).
- Comasco, E., Frokjaer, V. G. & Sundström-Poromaa, I. Functional and molecular neuroimaging of menopause and hormone replacement therapy. Front. Neurosci. 8, 388 (2014).

- 67. Grotzinger, H. et al. Diurnal fluctuations in steroid hormones tied to variation in intrinsic functional connectivity in a densely sampled male. *J. Neurosci.* **44**, e1856232024 (2024).
- 68. Dubol, M. et al. Acute nicotine exposure blocks aromatase in the limbic brain of healthy women: a ["C]cetrozole PET study. *Compr. Psychiatry* **123**, 152381 (2023).
- 69. Schmalenberger, K. M. et al. How to study the menstrual cycle: practical tools and recommendations. *Psychoneuroendocrinology* **123**, 104895 (2021).
- Bilió-Zulle, L. Comparison of methods: passing and Bablok regression. Biochem. Med. (Zagreb) 21, 49–52 (2011).
- Braun, V., Stuppner, H., Risch, L. & Seger, C. Design and validation of a sensitive multisteroid LC-MS/MS assay for the routine clinical use: one-step sample preparation with phospholipid removal and comparison to immunoassays. *Int. J. Mol. Sci.* 23, 14691 (2022).
- 72. Heller, C. et al. The ENIGMA-neuroendocrinology working group to bridge gaps in female mental health research. *Nat. Ment. Health* **2**, 348–350 (2024).

Publisher's note Springer Nature remains neutral with regard to jurisdictional claims in published maps and institutional affiliations.

Open Access This article is licensed under a Creative Commons Attribution 4.0 International License, which permits use, sharing, adaptation, distribution and reproduction in any medium or format, as long as you give appropriate credit to the original author(s) and the source, provide a link to the Creative Commons licence, and indicate if changes were made. The images or other third party material in this article are included in the article's Creative Commons licence, unless indicated otherwise in a credit line to the material. If material is not included in the article's Creative Commons licence and your intended use is not permitted by statutory regulation or exceeds the permitted use, you will need to obtain permission directly from the copyright holder. To view a copy of this licence, visit https://creativecommons.org/licenses/by/4.0/.

© The Author(s) 2025

Department of Psychiatry and Psychotherapy, Jena University Hospital, Jena, Germany. Masonic Institute for the Developing Brain, University of Minnesota, Minneapolis, MN, USA. ³Department of Pediatrics, University of Minnesota, Minneapolis, MN, USA. ⁴Department of Psychological and Brain Sciences, University of California, Santa Barbara, Santa Barbara, CA, USA. 5German Center for Mental Health (DZPG), Jena-Magdeburg-Halle, Germany. ⁶Center for Intervention and Research on Adaptive and Maladaptive Brain Circuits Underlying Mental Health (C-I-R-C), Jena–Magdeburg–Halle, Germany. ⁷Medical Physics Group, Institute of Diagnostic and Interventional Radiology, Jena University Hospital, Jena, Germany. ⁸Department of Psychiatry, University of Pennsylvania, Philadelphia, PA, USA. 9Department of Psychiatry and Behavioral Sciences, University of Minnesota, Minneapolis, MN, USA. 10 Institute of Neuroscience and Medicine (INM-7: Brain & Behaviour), Research Centre Jülich, Jülich, Germany. 11 Lab for Autonomic Neuroscience, Imaging and Cognition (LANIC), Department of Psychosomatic Medicine and Psychotherapy, Jena University Hospital, Jena, Germany. 12cBRAIN, Department of Child and Adolescent Psychiatry, Psychosomatics, and Psychotherapy, Ludwig-Maximilians-University, Munich, Germany. 13 Psychiatry Neuroimaging Laboratory, Department of Psychiatry, Brigham and Women's Hospital, Harvard Medical School, Boston, MA, USA. 14 Department of Psychiatry and Neurosciences, Charité - Universitätsmedizin Berlin, corporate member of Freie Universität Berlin and Humboldt-Universität zu Berlin, Berlin, Germany. 15 Institute of Child Development, Univeristy of Minnesota, Minneapolis, MN, USA. 16 Big Data Institute, Li Ka Shing Centre for Health Information and Discovery, Nuffield Department of Population Health, University of Oxford, Oxford, UK. 17Department of Statistics, University of Oxford, Oxford, UK. 18Oxford University Centre for Integrative Neuroimaging, FMRIB, Nuffield Department of Clinical Neurosciences, University of Oxford, Oxford, UK. ¹⁹Department of Clinical Psychology, Friedrich Schiller University Jena, Jena, Germany. ²⁰Department of Neurology, Jena University Hospital, Jena, Germany. 21 Institute of Clinical Chemistry and Laboratory Diagnostics, Jena University Hospital, Jena, Germany. 22 Neuroscience Research Institute, University of California, Santa Barbara, Santa Barbara, CA, USA. 23 Department of Psychotherapy and Psychosomatic Medicine, University Hospital Carl Gustav Carus, Technische Universität Dresden, Dresden, Germany. 24These authors contributed equally: Carina Heller, Daniel Güllmar.

⊠e-mail: carina.heller@uni-jena.de

Methods

Dense sampling, longitudinal datasets were acquired from three female participants in Jena, Germany. These datasets are referred to as the 'endometriosis cycle', 'typical cycle' and the 'OC cycle'. To extend our findings, we also leveraged the open-access 28andMe dataset of one female, which probes the extent to which endogenous fluctuations in sex hormones across a complete reproductive cycle influence the brain^{33–38,40}. The data were acquired in Santa Barbara, California, and are referred to as '28andMe (typical) cycle'.

For the purposes of control analyses and to probe comparability of our findings, an additional dense sampling, longitudinal dataset of one male was acquired over the time course of 5 weeks in Jena, Germany.

All participants (n = 5) gave written informed consent. The Friedrich Schiller University Jena Ethics Committee (for participants acquired in Jena) and the University of California, Santa Barbara Human Subjects Committee (for participants acquired in Santa Barbara) approved the study. Participants were not compensated. All imaging data are openly available.

Participants

Primary analyses. The study procedures for the participants in Jena, Germany, were as follows: the first healthy female (37 years of age, Caucasian) underwent most weekday testing for five consecutive weeks (9 January-12 February 2023) while freely cycling, resulting in 25 test sessions. The female participant ('typical cycle') had a history of regular menstrual cycles (last half-year mean length = 27.1 days, s.d. = 0.64, range = 26-28 days), no history of psychiatric, neurological and endocrine diagnoses, breastfeeding or pregnancy, and no history of alcohol or drug abuse, but the current use of nicotine. The second female participant (30 years of age, Caucasian) diagnosed with endometriosis ('endometriosis cycle') participated in this dense sampling, longitudinal study. She received the diagnosis 7 months before the assessments (28 October 2022) after a cyst surgery in the pelvic area. The participant was tracking her menstrual cycle length and reported a mean menstrual cycle length of 24.4 days (s.d. = 1.67, range = 23-27 days) during that time. Otherwise, the female participant had no history of psychiatric or neurological disorders, breastfeeding or pregnancy, and no history of smoking, alcohol or drug abuse. The participant underwent testing from Monday to Friday for five consecutive weeks (12 June–14 July 2023) while freely cycling, resulting in 25 test sessions. The third healthy female (31 years of age, Caucasian) underwent most weekday testing for five consecutive weeks (27 March-28 April 2023), resulting in 25 test sessions. Before the assessments, the participant had been prescribed a combined OC pill (0.03-mg ethinyl-estradiol, 2-mg dienogest, Maxim, Jenapharm) approximately 3 months before study initiation. The female participant ('OC cycle') had no history of psychiatric, neurological or endocrine diagnoses, nor had she experienced breastfeeding or pregnancy. Furthermore, she had no history of alcohol or drug abuse and did not use nicotine.

The study procedure for the fourth participant was as follows: a healthy female participant (23 years of age, Caucasian, '28andMe (typical) cycle') underwent testing for 30 consecutive days (9 July–7 August 2018) while freely cycling. She had a history of regular menstrual cycles (no missed periods, cycle occurring every 26–28 days) and had not taken hormone-based medication in the 12 months before the first study. The participant had no history of psychiatric or neurological disorders, breastfeeding or pregnancy, and no history of smoking, alcohol or drug abuse.

Additional analyses (male participant). The fifth participant, a healthy male (36 years of age, Caucasian), underwent most weekday testing for five consecutive weeks (4 May-7 June 2023), resulting in 25 test sessions. The male participant ('male') had no history of psychiatric, neurological or endocrine diagnoses, and reported no instances of alcohol, drug or nicotine abuse.

Image acquisition. For datasets collected in Jena (typical cycle, endometriosis cycle, OC, male), scans were collected at 7.30 a.m. (\pm 30 min) local time. The imaging dataset for the typical cycle was acquired on a 3 T MRI scanner (Prisma, Siemens Medical Solutions; software version MR E11) with a 64-channel head coil. The imaging datasets for the endometriosis cycle, male and female on OC, were acquired on a 3T MRI scanner (Prisma, Siemens Medical Solutions; software version MR XA30) with a 64-channel head coil. Structural MRI for the datasets was acquired with T1w magnetization prepared—rapid gradient echo sequence with the generalized autocalibrating partially parallel acquisitions acceleration. Scan parameters were as follows: echo time = 2.22 ms, repetition time = 2,400 ms, inversion time = 1,000 ms, flip angle = 8°, matrix size = 320 × 320 pixels, field of view = 256 mm, band width = 220 Hz pixel $^{-1}$ and slice thickness = 0.80 mm.

For the 28andMe (typical) cycle dataset, scans were collected on a 3 T MRI scanner (Prisma, Siemens Medical Solutions; software version MR D13D) equipped with a 64-channel head coil. Structural scans were acquired using a T1w magnetization prepared–rapid gradient echo sequence with the generalized autocalibrating partially parallel acquisitions acceleration with the following parameters: echo time = 2.31 ms, repetition time = 2,500 ms, inversion time = 934 ms, flip angle = 7° , matrix size = 320×320 pixels, field of view = 255 mm, band width = 210 Hz pixel $^{-1}$ and slice thickness = 0.80 mm.

Image preprocessing. The parameters used to acquire the images (for example, sizes, space directions and space origin) and the quality of the images (for example, motion artifacts, ringing, ghosting of the skull or eyeballs, cutoffs, signal drops and other artifacts) were visually inspected. One scan from the endometriosis cycle (test day 8) had to be removed due to artifacts in subcortical structures, corpus callosum and cingulate gyrus (measurements from this test day were excluded for all statistical analyses). The final datasets consisted of 24 T1w images for the endometriosis cycle, 25 T1w images for the typical cycle, 25 T1w images for the 28andMe (typical) cycle and 25 T1w images for the male.

The T1w images were converted from DICOM to NIfTI files using dcm2niix (version v1.0.20170724, https://www.nitrc.org/projects/ mricrogl/) and then preprocessed in SPM12 (version r7771, http:// www.fil.ion.ucl.ac.uk/spm) and the CAT12 (version 12.9, https:// neuro-jena.github.io/cat)⁵⁵ toolbox using the (plasticity) longitudinal pipeline approach in Matlab (The MathWorks, version R2021b). All T1w images were corrected for bias-field inhomogeneities and initially tissue-classified into gray matter, white matter and cerebrospinal fluid⁷³, followed by an adaptive maximum a posteriori segmentation⁷⁴, which also accounts for partial volume effects⁷⁵. The resulting gray and white matter partitions were spatially normalized to MNI space, Geodesic Shooting Registration⁷⁶. Subsequently, the normalized tissue segments were smoothed using a 6-mm full-width at half-maximum Gaussian Kernel. The extraction of cortical surfaces uses a projection-based thickness method⁷⁷ to estimate initial cortical thickness and central surface simultaneously. Topological defects are corrected using spherical harmonics⁷⁸, followed by surface refinement to produce final central, pial and white surface meshes. These surfaces refine the initial thickness measurement using the FreeSurfer metric⁷⁹. Subsequently, the individual central surfaces are aligned to the Free-Surfer FsAverage template hemisphere, spherically inflated to mini $mize\,distortions^{80}\,and\,spherically\,registered\,using\,a\,two\text{-}dimensional$ DARTEL approach^{81,82}.

Image quality and motion assessment. We conducted a quality assessment of all T1w images using the Image Quality Rating tool (https://neuro-jena.github.io/cat12-help/). Image quality was evaluated based on assigned values, with ratings of 1 and 2 indicating (very) good image quality (grades A and B), while values around 5 and higher suggest problematic image quality (grades E and above). Notably, all

assessed images exhibited excellent to good quality (endometriosis cycle–M = 1.407, s.d. = 0.002; typical cycle–M = 1.471, s.d. = 0.002; 28andMe (typical) cycle–M = 1.480, s.d. = 0.002; OC cycle–M = 1.503, s.d. = 0.003; male–M = 1.469, s.d. < 0.001).

Furthermore, mean framewise displacement (FWD), derived from a 12-min resting-state functional scan acquired before the T1w scans, was extracted to indicate motion across the entire scan duration (approximately 55 min). The MRI protocol included a resting-state functional scan for all participants, except for the typical cycle (here the functional scan was replaced with a magnetic resonance spectroscopy scan). Mean FWD was extremely minimal across all participants (endometriosis cycle—M = 0.121 mm, s.d. = 0.009 mm; OC cycle—M = 0.098 mm, s.d. = 0.009 mm; male—M = 0.137 mm, s.d. = 0.011 mm; Supplementary Fig. 1). Mean FWD for the 28andMe (typical) cycle is found elsewhere 40 and did not exceed 0.150 mm.

Endocrine procedure. For the datasets acquired in Jena, Germany, a blood draw was immediately followed by the MRI session at 8:30 a.m. (±30 min). One 4.9-ml blood sample was collected in an S-Monovette Serum-GEL (Sarstedt) with a clotting activator/gel at each test session. The sample was clotted at room temperature and centrifuged (2,500g for 10 min) within 2 h. Estradiol (pmol l⁻¹), luteinizing hormone (LH; IU I⁻¹), follicle-stimulating hormone (FSH; IU I⁻¹) and progesterone serum concentrations (nmol l⁻¹) were determined at the Institute of Clinical Chemistry and Laboratory Diagnostics, Jena University Hospital. Estradiol was assessed with the electrochemiluminescence immunoassay (ECLIA) Elecsys Estradiol III Assay. Assay antibodies, measuring ranges (defined by the limit of detection and the maximum of the master curve) and intra-assay precision coefficients of variation for estradiol were as follows: antibodies, two biotinylated monoclonal anti-estradiol antibodies (rabbit), 2.5 ng ml⁻¹ and 4.5 ng ml⁻¹; measuring range, 18.4-11,010 pmol l⁻¹ (5-3,000 pg ml⁻¹); intra-assay precision, ≤8.4% variation coefficient. LH was assessed with the ECLIA Elecsys LH Assay. Assay antibodies, measuring ranges and intra-assay coefficients of variation for LH were as follows: antibodies, biotinylated monoclonal anti-LH antibody (mice), 2.0 mg l⁻¹; measuring range, 0.3–200 mIU ml⁻¹ $(0.3-200 \text{ IU } \text{I}^{-1})$; intra-assay precision, $\leq 2.2\%$ variation coefficient. FSH was assessed with the ECLIA Elecsys FSH Assay. Assay antibodies, measuring ranges and intra-assay coefficients of variation for FSH were as follows: antibodies, biotinylated monoclonal anti-FSH antibody (mice), $0.5 \,\mathrm{mg}\,\mathrm{l}^{-1}$; measuring range, $0.3-200 \,\mathrm{mIU}\,\mathrm{ml}^{-1}(0.3-200)$ IU I^{-1}); intra-assay precision, $\leq 2.1\%$ variation coefficient. Progesterone was assessed with the ECLIA Elecsys Progesterone III Assay. Assay antibodies, measuring ranges and intra-assay coefficients of variation for progesterone were as follows: antibodies, biotinylated monoclonal antiprogesterone antibody (recombinant sheep), 30 ng ml⁻¹; measuring range, 0.159-191 nmol $l^{-1}(0.05-60 \text{ ng ml}^{-1})$; intra-assay precision, ≤20.7% variation coefficient. All assays were determined on the cobas e 402/801 analyzer (Roche Diagnostics GmbH) and were used according to the manufacturer's instructions. The reported intra-assay precision and coefficient of variation values are taken from the manufacturer's package inserts and reflect the analytical performance of the assays. These values are based on Roche's validation studies and do not represent quality control data generated at the Institute of Clinical Chemistry and Laboratory Diagnostics, Jena University Hospital, Jena, Germany.

For the 28 and Me (typical) cycle dataset acquired in Santa Barbara, CA, USA, a licensed phlebotomist inserted a saline-lock intravenous line into the dominant or nondominant hand or forearm. One 10-ml blood sample was collected in a vacutainer SST (BD Diagnostic Systems) each session. The sample was clotted at room temperature for 45 min until centrifugation (2,000g for 10 min) and then aliquoted into three 1-ml microtubes. Serum samples were stored at $-20\,^{\circ}\mathrm{C}$ until assayed. Serum concentrations were determined at the Brigham and Women's Hospital Research Assay Core. Estradiol and progesterone were assessed through LC-MS. Assay sensitivities, dynamic range

and intra-assay coefficients of variation (respectively) were as follows: estradiol-1 pg ml $^{-1}$, 1–500 pg ml $^{-1}$, <5% relative s.d.; progesterone-0.05 ng ml $^{-1}$, 0.05–10 ng ml $^{-1}$, 9.33% relative s.d. FSH and LH levels were determined using chemiluminescent assay (Beckman Coulter). The assay sensitivity, dynamic range and intra-assay coefficient of variation were as follows: FSH-0.2 mlU ml $^{-1}$, 0.2–200 mlU ml $^{-1}$, 3.1–4.3%; LH-0.2 mlU ml $^{-1}$, 0.2–250 mlU ml $^{-1}$, 4.3–6.4%.

Analysis approach. Please note that measurements from test day 8 of the endometriosis cycle were excluded from all statistical analyses to ensure consistency in the number of test days across all analyses.

Hormone concentrations. Statistical analyses of hormone concentrations were performed using Statistical Package for Social Sciences (SPSS; version 27). First, a one-way multivariate analysis of variance was conducted with estradiol levels, progesterone levels and estradiol-to-progesterone ratio as dependent variables. The fixed factors were the four individuals (endometriosis cycle, OC cycle, typical cycle and 28andMe (typical) cycle). Post hoc analyses of variance and two-tailed *t*-tests were performed and Bonferroni-corrected.

Structural brain measures. First, SVD was used to extract spatiotem-poral patterns from the preprocessed images by decomposing the three-dimensional image sets into spatial patterns (spatial component) and their associated temporal dynamics (time course and temporal component). The spatial patterns represent the brain regions that share similar spatial changes, while the temporal component reflects these changes evolve over time. To ensure consistency in spatial patterns while allowing for distinct temporal patterns, the typical cycle, the 28andMe (typical) cycle, the endometriosis cycle and the OC cycle were modeled together by concatenating the data from these participants. For the male participants, who do not have a menstrual cycle, the SVD was performed separately to account for the unique dynamics.

By using SVD, we can identify and analyze these patterns, revealing coherent time courses across the brain rather than being restricted to an expected change over time. This approach is analogous to applying independent component analysis to resting-state functional MRI data. However, while the motivation here is to identify underlying independent processes or networks, the objective of our study was to decompose the structural data into orthogonal (nonoverlapping) components. Furthermore, SVD provides consistent and repeatable patterns, which are crucial for reproducibility of the results across different datasets.

Using a flexible modeling approach, we assessed the variations in whole-brain volumetric and CSTPs across the monthly period. Specifically, we used a GAM using the 'mgcv' package (version 1.9-1) in RStudio (version 2024.04.1 + 748), which allows the independent variable (test days) to influence the outcome through smooth, nonlinear functions, to address potential nonlinear effects in volumetric and cortical thickness brain dynamics. The default value of k = 10 was used to determine the smoothness of the functions. This approach acknowledges the anticipated complexity and nonlinearity of the relationship between the menstrual cycle and brain structure, enabling a more adaptable modeling of menstrual cycle-dependent trajectories in structural brain dynamics. Initially, we also considered models with autoregressive terms to account for potential temporal dependencies in the data. However, model checks indicated that including autoregressive terms led to overfitting. There, we opted for the simpler GAM model, which provided a more reliable and interpretable fit. The following GAMs were fitted for the VSTPs for each individual separately:

$$VSTP1 = \beta_0 + f_1(\text{test day})$$

$$VSTP2 = \beta_0 + f_1(\text{test day})$$

$$VSTP3 = \beta_0 + f_1(\text{test day})$$

The following GAMs were fitted for the CSTPs for each individual separately (CSTP3 in the male only):

$$CSTP1 = \beta_0 + f_1(\text{test day})$$

$$CSTP2 = \beta_0 + f_1(\text{test day})$$

$$CSTP3 = \beta_0 + f_1(\text{test day})$$

GAMs were adjusted for multiple comparisons using the FDR method⁸³. Next, we assessed the relationship between the dynamics of volumetric and cortical thickness and gonadal hormones. To stabilize variances, gonadal hormone levels were transformed using the square root. We then used time-series regression models with VSTPs and CSTPs as dependent variables and the gonadal hormones as predictors in SPSS (version 27). These models captured the relationship between current structural dynamics and current gonadal hormone concentrations. The following time-series regression models were fitted for the VSTP1 for each individual separately:

$$VSTP1 = \beta_0 + \beta_1 \times \text{estradiol} + \varepsilon$$

$$VSTP1 = \beta_0 + \beta_1 \times \text{progesterone} + \varepsilon$$

$$VSTP1 = \beta_0 + \beta_1 \times \text{ratio} + \varepsilon$$

The same time-series regression models were fitted for VSTP2 and VSTP3, as well as CSTP1 and CSTP2 for each individual separately (CSTP3 in the male only). Additionally, we explored functional regression analyses incorporating autoregressive terms to account for potential dependencies in the data. However, model checks indicated that including autoregressive terms resulted in overfitting. As a result, we decided to use the initial simpler model without these terms. Finally, because not all variables were normally distributed, relationships were further investigated using nonparametric Spearman rank correlation, as implemented in the 'stats' package (version 4.4.0) in RStudio (version 2024.04.1 + 748). Results were highly consistent across both approaches. All models were adjusted for multiple comparisons using the FDR method⁸³.

Finally, to investigate the association between hormonal concentrations and structural brain measures at each voxel or vertex, we performed a statistical analysis using a general linear model in CAT12. Hormonal concentrations were included as the dependent variable in a regression framework. To identify statistically significant effects, we used the threshold-free cluster enhancement method (https://neuro-jena.github.io/software.html#tfce) 84 , which integrates both the magnitude and spatial extent of effects and controls for multiple comparisons by applying a family-wise error correction with a significance threshold of $P\!<\!0.01$. For voxel-wise analyses, voxels with an absolute threshold below 0.1 were excluded to focus exclusively on gray matter regions.

Reporting summary

Further information on research design is available in the Nature Portfolio Reporting Summary linked to this article.

Data availability

The datasets generated in Jena, Germany, are available at https://openneuro.org/datasets/ds006491. The dataset generated in Santa Barbara, CA, USA, is available at https://openneuro.org/datasets/ds002674. Source data are provided with this paper.

Code availability

Code is available in a public repository and can be found online at https://github.com/ChristianGaser/menstrual-brain-structural-dynamics.

References

- Ashburner, J. & Friston, K. J. Unified segmentation. Neuroimage 26, 839–851 (2005).
- Rajapakse, J. C., Giedd, J. N. & Rapoport, J. L. Statistical approach to segmentation of single-channel cerebral MR images. *IEEE Trans. Med. Imaging* 16, 176–186 (1997).
- 75. Tohka, J., Zijdenbos, A. & Evans, A. Fast and robust parameter estimation for statistical partial volume models in brain MRI. *Neuroimage* **23**, 84–97 (2004).
- 76. Ashburner, J. & Friston, K. J. Diffeomorphic registration using geodesic shooting and Gauss-Newton optimisation. *Neuroimage* **55**, 954-967 (2011).
- 77. Dahnke, R., Yotter, R. A. & Gaser, C. Cortical thickness and central surface estimation. *Neuroimage* **65**, 336–348 (2013).
- Yotter, R. A., Dahnke, R., Thompson, P. M. & Gaser, C. Topological correction of brain surface meshes using spherical harmonics. *Hum. Brain Mapp.* 32, 1109–1124 (2011).
- 79. Masouleh, S. K. et al. Influence of processing pipeline on cortical thickness measurement. *Cereb. Cortex* **30**, 5014–5027 (2020).
- Yotter, R. A., Thompson, P. M. & Gaser, C. Algorithms to improve the reparameterization of spherical mappings of brain surface meshes. J. Neuroimaging 21, e134–e147 (2011).
- 81. Ashburner, J. A fast diffeomorphic image registration algorithm. *Neuroimage* **38**, 95–113 (2007).
- 82. Yotter, R. A., Ziegler, G., Thompson, P. M. & Gaser, C. Diffeometric anatomical registration on the surface. Poster presented at the 17th annual meeting of the organization of human brain mapping, Quebec, Canada, 26–30 June 2011.
- 83. Benjamini, Y. & Hochberg, Y. Controlling the false discovery rate: a practical and powerful approach to multiple testing. *J. R. Stat. Soc. Series B Methodol.* **57**, 289–300 (1995).
- 84. Smith, S. M. & Nichols, T. E. Threshold-free cluster enhancement: addressing problems of smoothing, threshold dependence and localisation in cluster inference. *Neuroimage* **44**, 83–98 (2009).

Acknowledgements

This work was supported by the German Research Foundation (grant 544183227 to C.H.), the Interdisciplinary Center of Clinical Research of the Medical Faculty Jena (to L.C.), the National Institutes of Health (ROOMH127293 to B.L.), the Wellcome Trust Collaborative Award (215573/Z/19/Z to F.J.L.) and the Marie Skłodowska-Curie Innovative Training Network (SmartAge 859890 H2020-MSCA-ITN2019 to C.G.). The present work is endorsed by the German Center for Mental Health. The funders had no role in the study design, data collection, analysis and interpretation of data, or the writing of this manuscript.

Author contributions

C.H. was responsible for conceptualization, methodology, formal analysis, investigation, visualization, project administration, funding acquisition and writing the original draft of the manuscript. D.G. contributed to investigation, resources, data curation and writing (review and editing). L.C. contributed to investigation and writing (review and editing). L.P. contributed to investigation and writing (review and editing). M.G. contributed to formal analysis and writing (review and editing). N.J., F.d.l.C. and P.R. contributed to writing (review and editing). C.J.K. contributed to investigation and writing (review and editing). B.L. contributed to methodology and writing (review and editing). H.G. and F.J.L. contributed to formal analysis and writing (review and editing). A.-C.B. and T.L.J. contributed to investigation and writing (review and editing). R.D. contributed to formal analysis and writing (review and editing). M.K. contributed to resources, formal analysis and writing (review and editing). E.G.J. contributed to supervision and writing (review and editing). Z.K. contributed to conceptualization and writing (review and editing). M.W. and I.C. contributed to conceptualization, methodology,

resources, supervision and writing (review and editing). C.G. contributed to formal analysis, resources, data curation, visualization, supervision and writing (review and editing).

Funding

Open access funding provided by Friedrich-Schiller-Universität Jena.

Competing interests

The authors declare no competing interests.

Additional information

Extended data is available for this paper at https://doi.org/10.1038/s41593-025-02066-2.

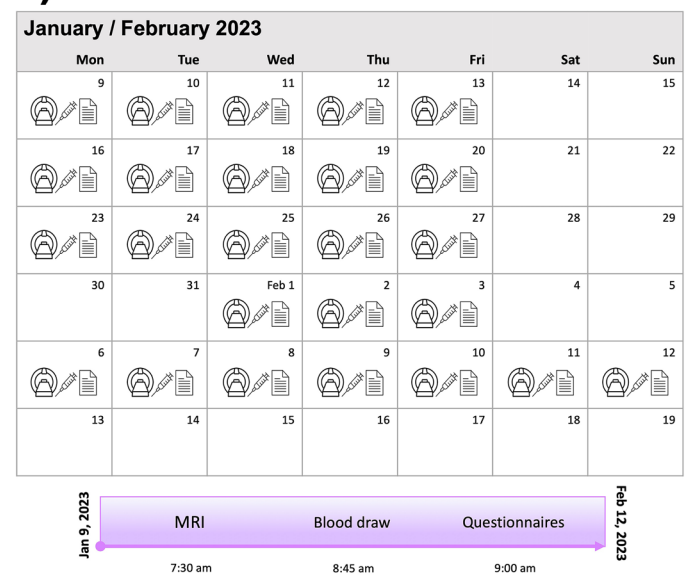
Supplementary information The online version contains supplementary material available at https://doi.org/10.1038/s41593-025-02066-2.

Correspondence and requests for materials should be addressed to Carina Heller.

Peer review information *Nature Neuroscience* thanks Jessica Bernard, Evan Gordon and the other, anonymous, reviewer(s) for their contribution to the peer review of this work

Reprints and permissions information is available at www.nature.com/reprints.

a) Typical cycle (n=1)

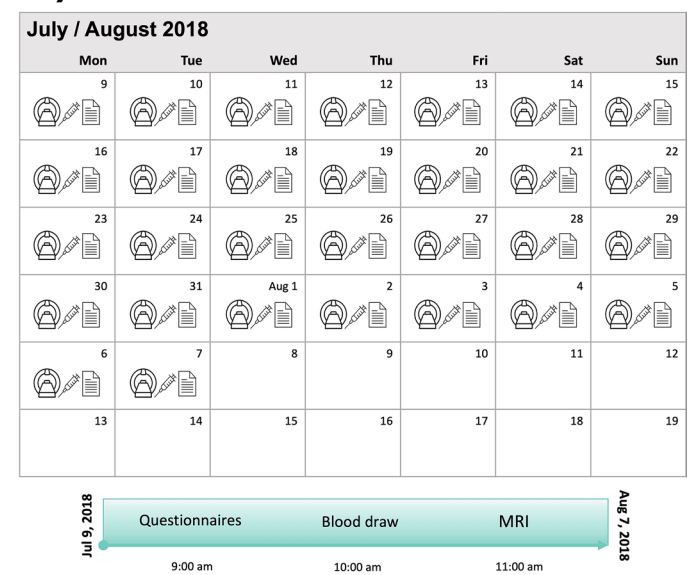


C) Endometriosis cycle (*n*=1)

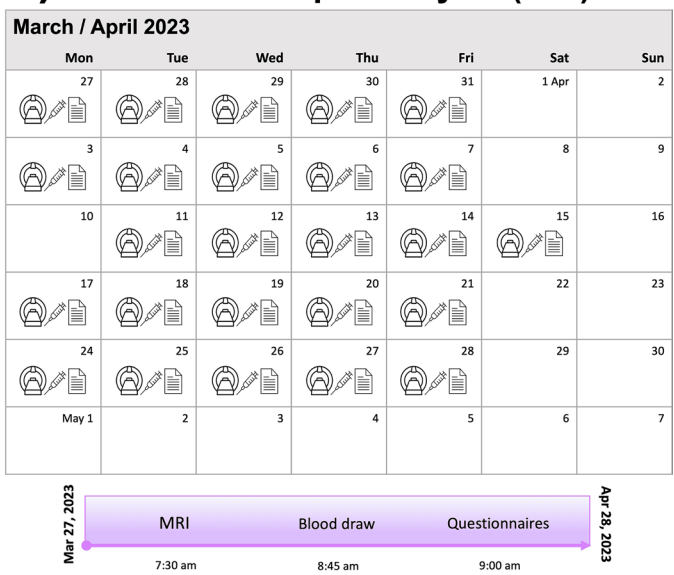
,				•	,	
June / Ju	ly 2023					
Mon	Tue	Wed	Thu	Fri	Sat	Sun
12	13	14	15	16	17	18
19	20	21	22	23	24	25
26	27	28	29	30	Jul 1	2
3	4	5	6	7	8	9
10	11	12	13	14	15	16
17	18	19	20	21	22	23
Jun 12, 2023	MRI		Blood draw	Ques	stionnaires	Jul 14, 2023
al 👇	7:30 an	1	8:45 am		9:00 am	023

Extended Data Fig. 1 | Timeline of the data collection for the female participants (n = 4). (a) The timeline of data collection for the typical cycle (n = 1). (b) The timeline of data collection for the 28 and Me (typical) cycle (n = 1). (c) The timeline of data collection for the endometriosis cycle (n = 1). (d) The timeline of data collection for the oral contraceptives cycle (n = 1). For (a-d) MRI

b) 28andMe (typical) cycle (n=1)



d) Oral contraceptives cycle (n=1)

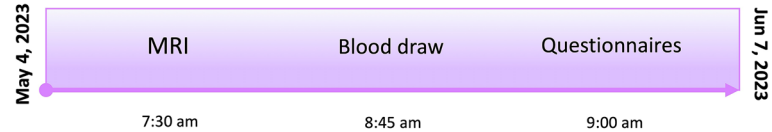


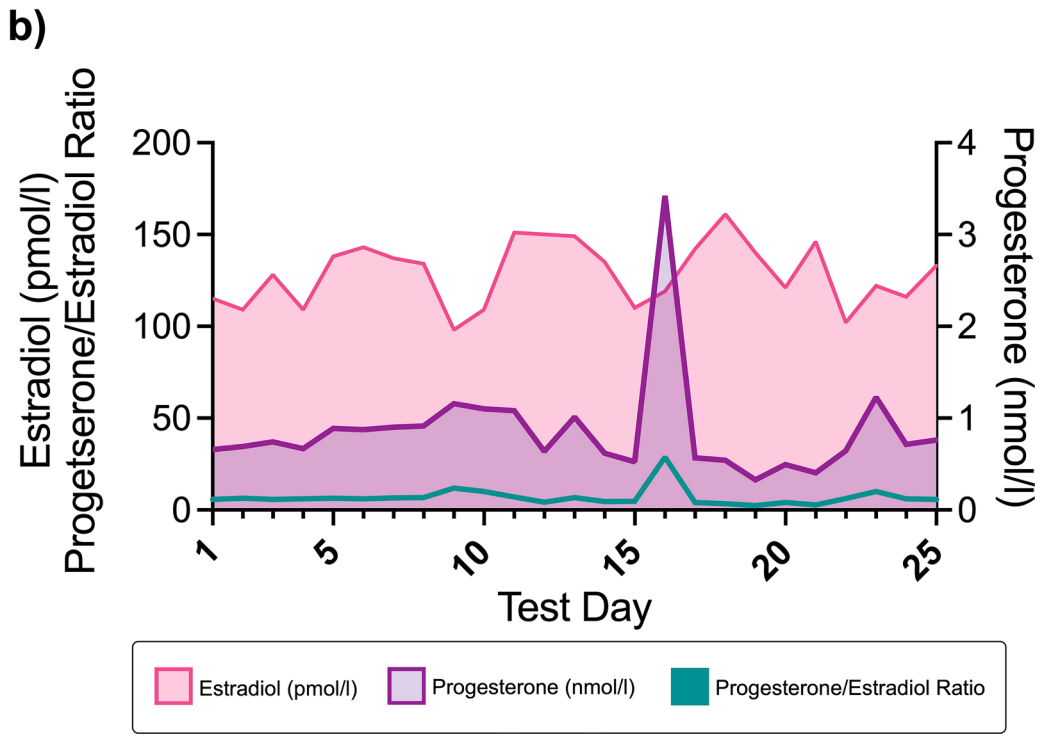
(MRI symbol), blood draw for hormonal assessments (syringe symbol), and mood questionnaires (paper symbol) were acquired simultaneously on each test day. Purple timeline bars represent the endometriosis cycle, the oral contraceptives cycle, and the typical cycle acquired in Jena, Germany. The turquoise timeline bar represents the 28 and Me (typical) cycle acquired in Santa Barbara, California, USA.

a)

Male (*n*=1)

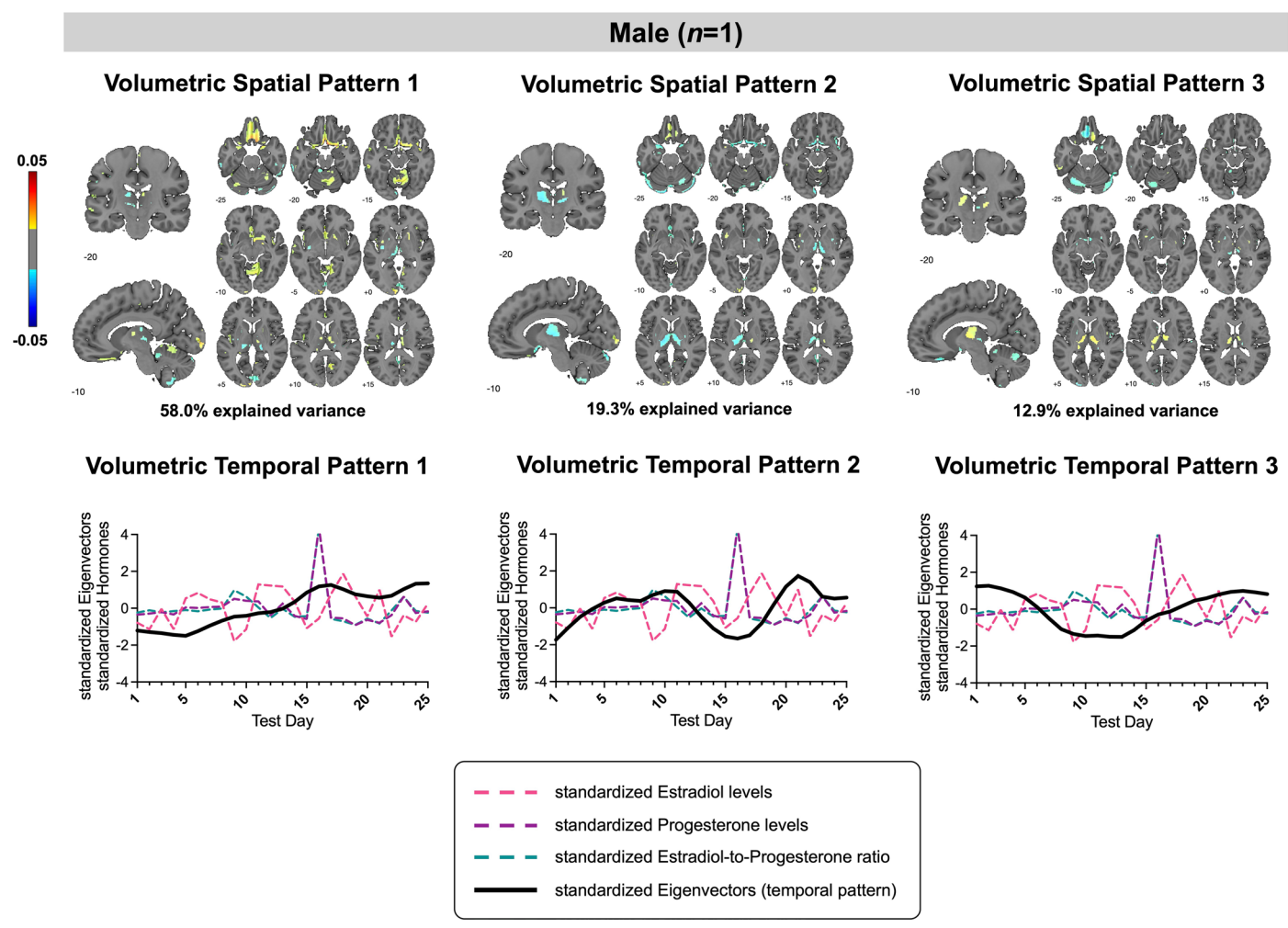
May / Jur	ne 2023					
Mon	Tue	Wed	Thu	Fri	Sat	Sun
1	2	3	4	5	6	7
8	9	10	11	12	13	14
15	16	17	18	19	20	21
22	23	24	25	26	27	28
29	30	31	Jun 1	2	3	4
5	6	7	8	9	10	11
2023	MRI		Blood draw	Quest	ionnaires	Jun 7





Extended Data Fig. 2 | Timeline of data collection and hormonal levels for the male participant (n=1). (a) The timeline of data collection for the male participant (n=1). MRI (MRI symbol), blood draw for hormonal assessments (syringe symbol), and mood questionnaires (paper symbol) were acquired simultaneously on each test day. Data was acquired in Jena, Germany. (b) The

hormonal levels of estradiol, progesterone, and the estradiol-to-progesterone ratio for the male participant across the five-week period. Solid lines and colored shaded areas represent hormonal levels. The male participant presented with anticipated low hormonal concentrations of estradiol, progesterone, and a low estradiol-to-progesterone ratio.



Extended Data Fig. 3 | Volumetric spatiotemporal patterns that significantly fluctuated in the male participant (n=1) across the five-week period. This figure depicts volumetric spatiotemporal patterns in the male participant that explained at least 10% of the variance. Spatial distribution of brain regions (top) and the associated temporal dynamics (bottom) of volumetric spatiotemporal pattern 1 (VSTP1), volumetric spatiotemporal pattern 2 (VSTP2) and volumetric spatiotemporal pattern 3 (VSTP3) are shown. Warm colors in the spatial maps indicate regions with positive associations to the temporal pattern (indicating regional volume increases as the temporal pattern increases). Cool colors in the spatial maps indicate negative associations to the temporal pattern (reflecting regional volume decreases as the temporal pattern increases). Spatial weights

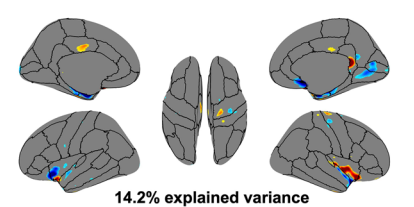
were thresholded, retaining only values within the ranges of -0.05 to -0.01 and 0.01 to 0.05, while excluding values between -0.01 and 0.01 that indicate minimal contribution to the respective spatial pattern (color bar). Solid black lines represent standardized eigenvectors (temporal pattern); dashed colored lines represent square-rooted and standardized hormonal values. Generalized additive models (GAMs) revealed that the volumetric spatiotemporal patterns fluctuated significantly across time. Time-series regressions revealed that the volumetric temporal patterns were not associated with hormonal levels in the male. For exact p-values, see Supplementary Table 10 and 11. Graphs were created using GraphPad Prism (version 10).

Male (n=1)

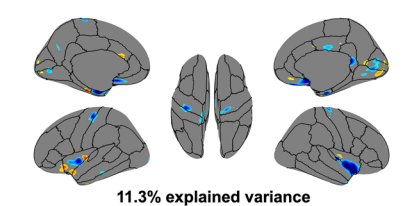
Cortical Thickness Spatial Pattern 1

0.02 40.2% explained variance

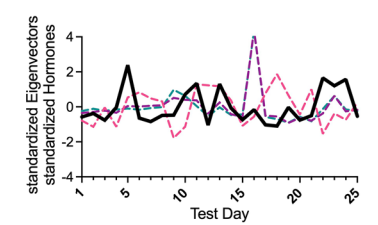
Cortical Thickness Spatial Pattern 2



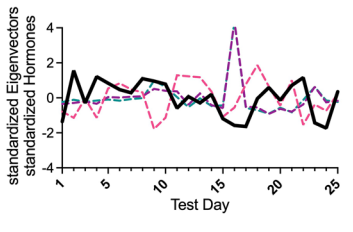
Cortical Thickness Spatial Pattern 3



Cortical Thickness Temporal Pattern 1

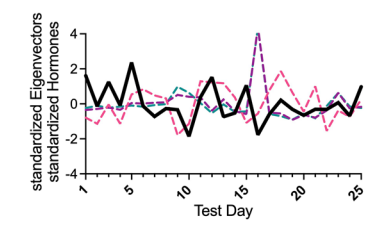


Cortical Thickness Temporal Pattern 2





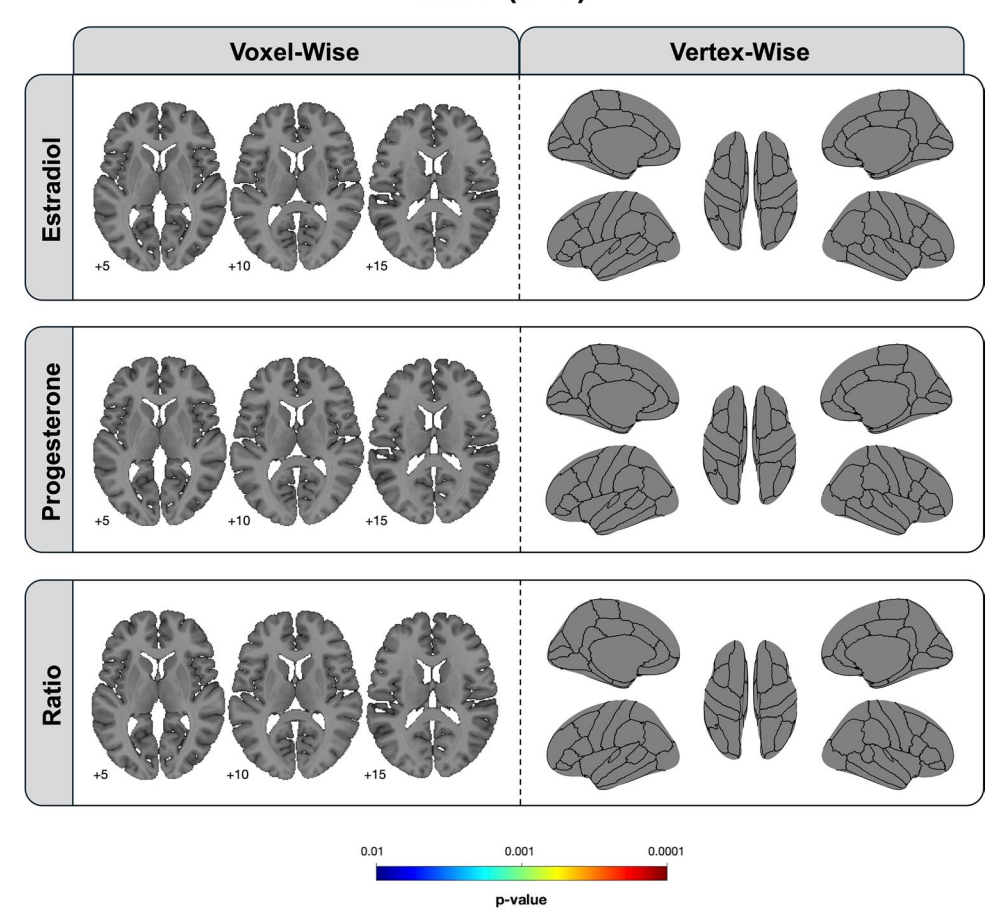
Cortical Thickness Temporal Pattern 3



Extended Data Fig. 4 | Cortical thickness spatiotemporal patterns in the male participant (n=1) across the five-week period. This figure depicts cortical thickness spatiotemporal patterns in the male participant that explained at least 10% of the variance. Spatial distribution of brain regions (top) and the associated temporal dynamics (bottom) of cortical thickness spatiotemporal pattern 1 (CSTP1), cortical thickness spatiotemporal pattern 2 (CSTP2) and cortical thickness spatiotemporal pattern 3 (CSTP3) are shown. Warm colors in the spatial maps indicate regions with positive associations to the temporal pattern (indicating regional cortical thickness increases as the temporal pattern increases). Cool colors in the spatial maps indicate negative associations to the temporal pattern (reflecting regional cortical thickness decreases as the

temporal pattern increases). Spatial weights were thresholded, retaining only those within the ranges of -0.02 to -0.01 and 0.01 to 0.02, while excluding values between -0.01 and 0.01 that indicate minimal contribution to the respective spatial pattern (color bar). Solid black lines represent standardized eigenvectors (temporal pattern); dashed colored lines represent square-rooted and standardized hormonal values. Generalized additive models (GAMs) revealed that the cortical thickness temporal patterns did not significantly fluctuate across the five-week period and time-series regressions revealed that they were not associated with hormonal levels in the male. For exact p-values, see Supplementary Table 10 and 11. Graphs were created using GraphPad Prism (version 10).

Male (*n*=1)



Extended Data Fig. 5 | Results from the voxel- and vertex-wise analyses in the male participant (n=1) across the five-week period. To directly link hormonal fluctuations to structural brain measures, complementary voxel- and vertex-wise analyses were also conducted using general linear models (GLMs) in the male participant as a sensitivity check with the Threshold-Free Cluster Enhancement (TFCE) method which controls for multiple comparisons by applying a family-

wise error (FWE) correction. No significant associations were found in the voxel-and vertex-wise analysis between structural brain measures (volume, cortical thickness) and hormone levels in males. Estradiol, square-rooted estradiol levels; progesterone, square-rooted progesterone levels; ratio, square-rooted estradiol-to-progesterone ratio.

nature portfolio

	Carina Heller, Friedrich Schiller University
Corresponding author(s):	Jena, Jena, Germany

Last updated by author(s): Aug 3, 2025

Reporting Summary

Nature Portfolio wishes to improve the reproducibility of the work that we publish. This form provides structure for consistency and transparency in reporting. For further information on Nature Portfolio policies, see our <u>Editorial Policies</u> and the <u>Editorial Policy Checklist</u>.

For all statistical analyses, confirm that the following items are present in the figure legend, table legend, main text, or Methods section.

\sim				•
⋖.	ヒつ	+	ıst	ICS
٠,				11 \

n/a	Cor	nfirmed
	\boxtimes	The exact sample size (n) for each experimental group/condition, given as a discrete number and unit of measurement
	\boxtimes	A statement on whether measurements were taken from distinct samples or whether the same sample was measured repeatedly
	\boxtimes	The statistical test(s) used AND whether they are one- or two-sided Only common tests should be described solely by name; describe more complex techniques in the Methods section.
\boxtimes		A description of all covariates tested
	\boxtimes	A description of any assumptions or corrections, such as tests of normality and adjustment for multiple comparisons
	\boxtimes	A full description of the statistical parameters including central tendency (e.g. means) or other basic estimates (e.g. regression coefficient) AND variation (e.g. standard deviation) or associated estimates of uncertainty (e.g. confidence intervals)
\boxtimes		For null hypothesis testing, the test statistic (e.g. <i>F</i> , <i>t</i> , <i>r</i>) with confidence intervals, effect sizes, degrees of freedom and <i>P</i> value noted <i>Give P values as exact values whenever suitable.</i>
\times		For Bayesian analysis, information on the choice of priors and Markov chain Monte Carlo settings
\boxtimes		For hierarchical and complex designs, identification of the appropriate level for tests and full reporting of outcomes
	\boxtimes	Estimates of effect sizes (e.g. Cohen's d, Pearson's r), indicating how they were calculated

$\textit{Our web collection on } \underline{\textit{statistics for biologists}} \textit{ contains articles on many of the points above}.$

Software and code

Policy information about availability of computer code

Data collection

The imaging dataset for the typical cycle was acquired on a 3T MRI scanner (Prisma, Siemens Medical Solutions, Erlangen, Germany) with software version MR E11.

The imaging datasets for the endometriosis cycle, male, and female on oral contraceptives were acquired on a 3T MRI scanner (Prisma, Siemens Medical Solutions, Erlangen, Germany) with software version MR XA30.

For the 28andMe (typical) cycle dataset, scans were collected on a 3T MRI scanner (Prisma, Siemens Medical Solutions, Erlangen, Germany) with software version MR D13D.

All protocols were standard Siemens protocols. No other custom software was used for data collection.

Data analysis

- RStudio (version 2024.04.1+748)
- 'mgcv' package (version 1.9-1)
- 'stats' package (version 4.4.0)
- Statistical Package for Social Sciences (SPSS) version 27
- dcm2niix (version v1.0.20170724)
- Matlab (The MathWorks Inc., Natick, MA, USA, version R2921b)
- SPM12 (http://www.fil.ion.ucl.ac.uk/spm, version r7771)
- CAT12 (https://neuro-jena.github.io/cat, version 12.9)

For manuscripts utilizing custom algorithms or software that are central to the research but not yet described in published literature, software must be made available to editors and reviewers. We strongly encourage code deposition in a community repository (e.g. GitHub). See the Nature Portfolio guidelines for submitting code & software for further information.

Data

Policy information about availability of data

All manuscripts must include a data availability statement. This statement should provide the following information, where applicable:

- Accession codes, unique identifiers, or web links for publicly available datasets
- A description of any restrictions on data availability
- For clinical datasets or third party data, please ensure that the statement adheres to our policy

Data availability: Datasets acquired in Jena, Germany, are available at https://openneuro.org/datasets/ds006491. The dataset acquired in Santa Barbara, CA, USA, is available at https://openneuro.org/datasets/ds002674.

Research involving human participants, their data, or biological material

Policy information about studies with <u>human participants or human data</u>. See also policy information about <u>sex, gender (identity/presentation)</u>, and sexual orientation and race, ethnicity and racism.

Reporting on sex and gender

In our manuscript we consistently use the terms "sex" and "female" and "male" to refer to our study population, as our central focus was on gonadal hormones as a biological varibale and how these hormones (estradiol and progesterone) impact brain structure. Sex of all participants was reported (4 females, 1 male).

Reporting on race, ethnicity, or other socially relevant groupings

In the method's section of our manuscript we report about the ethnicity of our participants, which was self reported by all participants. All subjects were white.

Population characteristics

All participants were of reproductive age (range: 23 - 37 years of age). Females recruited with a typical natural menstrual cycle (authors L.C. and L.P.) reported a regular menstrual cycle lengths (around approximately 28 days). The female diagnosed with endometriosis received the diagnosis seven months prior to the assessments (October 28, 2022) after a cyst surgery in the pelvic area. The participant was tracking her menstrual cycle length and reported a mean menstrual cycle length of 24.4 days (SD = 1.67, range = 23 – 27 days). The female on oral contraceptives (author C.H.) was using the regimen for at least three months prior to the assessment. Hormonal values for the male (author T.L.J.) were within the usual range for males. All participants reported no history of psychiatric and neurological disorders, breastfeeding or pregnancy, alcohol or drug abuse.

Recruitment

The female with endometriosis was recruited as a voluntary participant from the general population with the use of advertisements. The females with the natural menstrual cycles (authors L.C. and L.P.), the female on oral contraceptives (author C.H.), and the male (author T.L.J.) were recruited as volunteers from the Department of Clinical Psychology, Friedrich Schiller University Jena, Jena, Germany, and the Department of Psychiatry and Psychotherapy, Jena University Hospital, Jena, Germany, as well as the Department of Psycholoical and Brain Sciences, University of California Santa Barbara, Santa Barbara, CA, USA. The project was conceived by the authors to use themselves as participants, as has been done in previous "dense-sampling" studies (cf. Poldrack et al., 2015; Pritschet et al., 2020; Heller et al., 2024). Because the authors served as participants, there is a potential for self-selection bias, as they may not represent the general population. This limits generalizability but does not affect the internal validity of the dense-sampling, within-subject design.

Ethics oversight

All participants gave written informed consent. The Friedrich Schiller University Jena Ethics Committee (for participants acquired in Jena, Germany) and the University of California, Santa Barbara Human Subjects Committee (for participant acquired in Santa Barbara, USA) approved the study. Participants were not compensated.

Note that full information on the approval of the study protocol must also be provided in the manuscript.

Field-specific reporting

Please select the one belo	w that is the best fit for your research	i. If you are not sure, read the appropriate sections before making your selection.
X Life sciences	Behavioural & social sciences	Ecological, evolutionary & environmental sciences

For a reference copy of the document with all sections, see <u>nature.com/documents/nr-reporting-summary-flat.pdf</u>

Life sciences study design

All studies must disclose on these points even when the disclosure is negative.

Sample size

Sample size was N=5. No formal sample-size calculation was performed due to the single-subject design. Instead of collecting data from multiple individuals and then pooling the data to establish mean comparisons across groups, statistical power is achieved by following the same individual across a densely sampled time-scale (in our case four to five weeks). The number of test days was selected based on previously published dense-sampling studies investigating hormone-brain associations (cf Pritschet et al., 2020; Pritschet et al., 2024; Heller et al., 2024).

Endomtriosis cycle: n=1, 25 test days Typical cycle: n=1, 25 test days

(28andMe (typical) cycle: n=1, 30 test days
Oral contraceptives cycle: n=1, 25 test days
Male: n=1, 25 test days

Data exclusions

One structural MRI scan from one day needed to be excluded due to artifacts in the scan. This particular scan was the 8th scan within the dataset of the female with endometriosis. Measurements from that day were excluded for all statistical analyses. The final number of test days for analyses for the endometriosis cycle was 24 test days.

Replication

This is the first study of its kind, and as such, no direct replications currently exist. However, to assess the reproducibility of our findings—specifically, the associations between hormones and spatiotemporal brain patterns—we conducted voxel-wise and vertex-wise sensitivity analyses. Voxel-wise analyses revealed positive associations between brain volume and hormone concentrations that spatially overlapped with the patterns identified in the SVD analyses. Consistent with the SVD results, estradiol-related associations were most prominent in the endometriosis cycle, whereas progesterone-related associations were more evident in the typical cycles. Vertex-wise analyses similarly showed few associations between cortical thickness and hormone concentrations, in line with the SVD findings. As an additional sensitivity check, we repeated the SVD, voxel-wise, and vertex-wise analyses in a male participant; none of the analyses showed meaningful associations with hormone levels.

Randomization

Since this study consists of a single-subject design where participants were scanned repeatedly over the time course of five weeks and were not grouped for analyses, randomization and covariate analyses were not necessary.

Blinding

Blinding was not possible in this study because the authors also served as participants and were fully aware of the experimental conditions, cycle phases, and test days.

Reporting for specific materials, systems and methods

We require information from authors about some types of materials, experimental systems and methods used in many studies. Here, indicate whether each material, system or method listed is relevant to your study. If you are not sure if a list item applies to your research, read the appropriate section before selecting a response.

Ma	terials & experimental systems	Methods		
n/a	Involved in the study	n/a	Involved in the study	
	Antibodies	\boxtimes	ChIP-seq	
\boxtimes	Eukaryotic cell lines	\boxtimes	Flow cytometry	
\boxtimes	Palaeontology and archaeology		MRI-based neuroimaging	
\boxtimes	Animals and other organisms			
\boxtimes	Clinical data			
\boxtimes	Dual use research of concern			
\boxtimes	Plants			
	•			

Antibodies

Antibodies used

 $Anti-Estradiol-Ak^{\sim}Biotin, 19.7 \ mL: Two \ biotinylated \ monoclonal \ anti-Estradiol \ antibodies \ (rabbit), 2.5 \ ng/mL \ and 4.5 \ ng/mL; \\ Mesterolone, 130 \ ng/mL; \ MESb \ buffer, 50 \ mmol/L, pH 6.0; Preservative.$

Anti-Progesterone-Ak~Biotin, 21.0 mL: Biotinylated monoclonal anti-Progesterone antibody (recombinant, sheep), 30 ng/mL; Phosphate buffer, 25 mmol/L, pH 7.0; Preservative.

Anti-FSH-Ab~biotin, 10 mL: Biotinylated monoclonal anti@FSH antibody (mouse) 0.5 mg/L, MES buffer 50 mmol/L, pH 6.0; preservative.

Anti-FSH-Ab~Ru(bpy), 10 mL: Monoclonal anti@FSH antibody (mouse) labeled with ruthenium complex 0.8 mg/L, MES buffer 50 mmol/l, pH 6.0; preservative

Anti-LH-Ab~biotin, 10 mL: Biotinylated monoclonal anti@LH antibody (mouse) 2.0 mg/L; TRIS buffer 50 mmol/L, pH 8.0; preservative. Anti-LH-Ab~Ru(bpy), 10 mL: Monoclonal anti@LH antibody (mouse) labeled with ruthenium complex 0.3 mg/L; TRIS buffer 50 mmol/L, pH 8.0; preservative.

Validation

Hormone concentrations were measured using standardized electrochemiluminescence immunoassays (ECLIA) on the Roche cobas e platform:

- Electrochemiluminescence immunoassay (ECLIA) Elecsys® Estradiol III Assay (https://diagnostics.roche.com/global/en/products/lab/elecsys-estradiol-iii-cps-000466.html): measuring range, 18.4 11,010 pmol/l (5 3000 pg/ml); intra-assay precision, $\leq 8.4\%$ variation coefficient.
- Electrochemiluminescence immunoassay (ECLIA) Elecsys® Progesterone III Assay (https://diagnostics.roche.com/global/en/products/lab/elecsys-progesterone-iii-cps-000501.html): measuring range, 0.159 − 191 nmol/l (0.05 − 60 ng/ml); intra-assay precision, ≤ 20.7% variation coefficient.
- Electrochemiluminescence immunoassay (ECLIA) Elecsys® FSH Assay (https://diagnostics.roche.com/global/en/products/lab/elecsys-fsh-cps-000472.html): measuring range, 0.3 200 mlU/ml (0.3 200 lU/l); intra-assay precision, ≤ 2.1% variation coefficient.
- Electrochemiluminescence immunoassay (ECLIA) Elecsys® LH Assay (https://diagnostics.roche.com/global/en/products/lab/elecsys-lh-cps-000492.html): measuring range, 0.3 200 mIU/ml (0.3 200 IU/l); intra-assay precision, ≤ 2.2% variation coefficient.

All assays were determined on the cobas® e 402/801 analyzer (Roche Diagnostics GmbH, Mannheim, Germany) and were used according to the manufacturer's instructions. The reported intra-assay precision and coefficient of variation values are taken from the manufacturer's package inserts and reflect the analytical performance of the assays. These values are based on Roche's validation studies and do not represent quality control data generated at the Institute of Clinical Chemistry and Laboratory Diagnostics, Jena University Hospital, Jena, Germany.

Plants

Seed stocks

Report on the source of all seed stocks or other plant material used. If applicable, state the seed stock centre and catalogue number. If plant specimens were collected from the field, describe the collection location, date and sampling procedures.

Novel plant genotypes

Describe the methods by which all novel plant genotypes were produced. This includes those generated by transgenic approaches, gene editing, chemical/radiation-based mutagenesis and hybridization. For transgenic lines, describe the transformation method, the number of independent lines analyzed and the generation upon which experiments were performed. For gene-edited lines, describe the editor used, the endogenous sequence targeted for editing, the targeting guide RNA sequence (if applicable) and how the editor was applied.

Authentication

Describe any authentication procedures for each seed stock used or novel genotype generated. Describe any experiments used to assess the effect of a mutation and, where applicable, how potential secondary effects (e.g. second site T-DNA insertions, mosiacism, off-target gene editing) were examined.

Magnetic resonance imaging

Experimental design	
Design type	No task or resting-state MRI acquired
Design specifications	No task or resting-state MRI acquired
Behavioral performance measures	No task or resting-state MRI acquired
Acquisition	
Imaging type(s)	Structural MRI: T1-weighted (T1w) magnetization prepared - rapid gradient echo (MPRAGE) sequence with the generalized autocalibrating partially parallel acquisitions (GRAPPA) acceleration.
Field strength	ЗТ
Sequence & imaging parameters	Data from Jena: echo time (TE) = 2.22 ms, repetition time (TR) = 2400 ms, inversion time (TI) = 1000 ms, flip angle = 8° , matrix size = 320×320 pixels, field of view (FOV) = 256 mm, band width = 220 Hz/pixel, and slice thickness = 0.80 mm. Data from Santa Barbara: TE = 2.31 ms, TR = 2500 ms, TI = 934 ms, flip angle = 7° , matrix size = 320×320 pixels, FOV = 255 mm, band width = 210 Hz/pixel, and slice thickness = 0.80 mm.
Area of acquisition	Whole brain scan
Diffusion MRI Used	Not used ■

Preprocessing

Preprocessing software

The T1w images were converted from Dicom to Nifti files using dcm2niix (Chris Rorden, version v1.0.20170724, https://www.nitrc.org/projects/mricrogl/) and then preprocessed in SPM12 (https://www.fil.ion.ucl.ac.uk/spm) and the CAT12 (https://neuro-jena.github.io/cat) toolbox using the longitudinal pipeline approach in Matlab R2021b (The MathWorks Inc., Natick, MA, USA). All T1w images were corrected for bias-field inhomogeneities and initially tissue-classified into gray matter, white matter, and cerebrospinal fluid, followed by an adaptive maximum a posteriori segmentation, which also accounts for partial volume effects

Normalization

The resulting gray and white matter partitions were spatially normalized to MNI space Geodesic Shooting Registration.

Normalization template

MNI space Geodesic Shooting Registration

Noise and artifact removal

Please see above: One scan from the female with endometriosis had to be excluded due to artefacts within the corpus callosum and subcortical structures. All other T1-weighted images were corrected for bias-field inhomogeneities and tissue-classified into gray matter, white matter, and cerebrospinal fluid, which also included an approach accounting for partial volume effects by applying adaptive maximum a posteriori estimations and a hidden Markov Random Field Model.

Volume censoring

N/A

Statistical modeling & inference

Model type and settings

Singular Value Decomposition (SVD) was used to extract spatiotemporal patterns from the preprocessed images by decomposing the three-dimensional image sets into spatial patterns (maps) and their associated temporal dynamics (time

course) for each participant separately. The spatial patterns represent the regions of the brain that share a similar temporal pattern, while the temporal dynamics describe how the local volume of these regions changes over time. SVD analysis was performed for all female individuals combined (group-level). SVD analysis for the male was performed separately. The SVD analyses yielded more than one spatiotemporal patterns exceeding a threshold of 1.

Effect(s) tested

We assessed the variations in whole-brain volumetric and cortical thickness spatiotemporal patterns across the monthly period using general additive modeling (GAM). This approach acknowledges the anticipated complexity and nonlinearity of the relationship between the menstrual cycle and brain structure, allowing for a more adaptable modeling of menstrual cycle-dependent trajectories in structural brain dynamics. We then employed linear regression models with volumetric and cortical thickness spatiotemporal patterns as dependent variables and the gonadal hormones as predictors. Since not all variables were normally distributed, relationships were further modeled using non-parametric functional Spearman rank correlation. Results were highly consistent across both approaches. Furthermore, to account for possible autocorrelation, GAMs with an autogressive term and functional linear regressions with an autoregressive terms were calculated. Results were highly consistent across approaches with and without autoregressive terms. However, autoregressive terms led to overfitting of the model which supported our decision to use the simpler models.

To investigate the association between hormonal concentrations and structural brain measures at each voxel or vertex, statistical analysis using a general linear model (GLM) was performed. Hormonal concentrations were included as the dependent variable in a regression framework. To identify statistically significant effects, the Threshold-Free Cluster Enhancement (TFCE) method was used.

Specify type of analysis:	Whole brain ROI-based Both
Statistic type for inference	Voxel-wise, vertex-wise
(See Eklund et al. 2016)	
Correction	Corrected for multiple comparisons using False Discovery Rate (FDR) and Family-Wise Error (FWE).
Models & analysis	
n/a Involved in the study	

/a	Involved in the study
\times	Functional and/or effective connectivity
\times	Graph analysis
\times	Multivariate modeling or predictive analys